Integrated Luminal and Cytosolic Aspects of the Calcium Release Control

Irina Baran
Biophysics Department, Faculty of Medicine, "Carol Davila" University of Medicine and Pharmacology, 76241 Bucharest, Romania

ABSTRACT We propose here a unitary approach to the luminal and cytosolic control of calcium release. A minimal number of model elements that realistically describe different data sets are combined and adapted to correctly respond to various physiological constraints. We couple the kinetic properties of the inositol 1,4,5 trisphosphate receptor/calcium channel with the dynamics of Ca^{2+} and K^+ in both the lumen and cytosol, and by using a detailed simulation approach, we propose that local (on a radial distance $\sim 2\ \mu$m) calcium oscillations in permeabilized cells are driven by the slow inactivation of channels organized in discrete clusters composed of between six and 15 channels. Moreover, the character of these oscillations is found to be extremely sensitive to K^+, so that the cytosolic and luminal calcium variations are in or out of phase if the store at equilibrium has tens or hundreds μM Ca^{2+}, respectively, depending on the K^+ gradient across the reticulum membrane. Different patterns of calcium signals can be reproduced through variation of only a few parameters.

INTRODUCTION

Release of calcium ions from specialized compartments is a key process in numerous cellular events (Berridge, 1993; Clapham,1995). The complex nature of intracellular calcium dynamics relies on the interplay between specifically induced calcium fluxes, such as release from the endo- or sarcoplasmic reticulum through the inositol 1,4,5 trisphosphate (IP_3) receptor or the ryanodine receptor (RyR), uptake by the endoplasmic reticulum (ER) through the smooth ER Ca^{2+} pump, or calcium influx from the outside through Ca^{2+} channels on the plasma membrane, among which store-operated calcium channels are thought to directly sense the ER calcium content. Exchange with mitochondria plays also a significant role in preventing prolonged increases in cytosolic Ca^{2+} (Hajnóczky et al., 1999).

Nevertheless, the coupled control on both channel gating and store filling plays the key role in shaping cytosolic calcium signals. Studies on the IP_3 receptor/Ca^{2+} channel in its native environment or reconstituted into lipid bilayers have revealed a biphasic effect of Ca^{2+} on the channel, given by ion binding to antagonist—activating/inhibitory—classes of sites, whereas IP_3's binding properties and effects have received various interpretation. The global picture is even more complexed by parallel variations of the intraluminal source of calcium during release. The ER is known to have a high buffering capacity for Ca^{2+}, but little is known about the exact dynamics and role, either direct or indirect, of store filling in calcium signaling. Recently an important feature of calcium release regulation has been characterized (Nguyen et al., 1998) through direct involvement of potassium ions toward mobilization of Ca^{2+} from the luminal matrix. Moreover, besides the dynamic Ca^{2+}/K^+ exchange during release, there exists the additional possibility of a direct effect of luminal calcium at the receptor level. Although this mechanism gained convincing evidence (Györke and Györke, 1998) in the case of the RyR, the corresponding effect on the IP_3 receptor (IP_3R) still awaits clarification (Taylor and Traynor, 1995).

The many facets of intracellular calcium signaling (Berridge et al., 2000) have proved to be rather difficult to incorporate into a consistent, unitary description. Different proposed models (see Dupont, 1999, for review) involving calcium release properties are able to explain quantal release or incremental detection when applied to permeabilized cell-like conditions, but cannot reproduce IP_3-induced oscillations unless applied to intact cell-like conditions, where a conservation rule is generally used for intracellular calcium. The few current quantitative models (De Young and Keizer, 1992; Bezprozvanny and Erlich, 1994; Kaftan et al., 1997; Swillens et al., 1998; Moraru et al., 1999; Swillens et al., 1999) on regulation of IP_3R activity have been mainly used to explain the Ca^{2+} and IP_3 dependence of the steady-state open probability, or to simulate Ca^{2+} release at discrete sites, at constant luminal or cytosolic Ca^{2+}. Moreover, these models are based on data obtained with channels incorporated into reconstituted bilayers, which are quantitatively largely different from data on the outer nuclear membrane.

The present study explores a new dimension of the calcium release dynamics and intends to answer two main questions: 1), to what extent can calcium signals depend on K^+, and 2), how can in- or out-of-phase local calcium oscillations be explained in permeabilized cells? To this end we construct a basis for quantifying the dynamical relation between store and cytosolic calcium by coupling it to the IP_3R/Ca^{2+} channel kinetics and to the control of the luminal calcium content by potassium. The model we propose here is based on the derivation of basic parameters that define both Ca^{2+}/K^+ exchange inside the store and gating properties of

Submitted April 16, 2002, and accepted for publication October 8, 2002.
Address reprint requests to Irina Baran, Bd. Eroii Sanitari 8, 76241 Bucharest, Romania. Tel.: 040-21-3125955; Fax: 040-21-3125955; E-mail: baran@theorl.theory.nipne.ro.

0006-3495/03/03/1470/16 $2.00

the ER calcium channel in nuclear membranes. With these parameters in hand, we simulate Ca^{2+} release through a cluster of channels in cylindrical geometry, taking into consideration ion diffusion and binding to endo- and exogenous buffers within the lumen and cytosol, in conditions that reproduce the main features of the physiologic subcellular environment. The model accurately describes a series of disparate experimental data that have not been theoretically considered to the moment and gives a more complete and detailed simulation approach to the calcium release process than previously done. Various approximations currently used (such as buffering approximations, spherical symmetry, constant luminal Ca^{2+}, constant channel current, and neglect of intraluminal ion diffusion) are replaced here by direct approach to the underlying phenomena.

We discuss two possible scenarios for the K^+ role in calcium release and show that the previously proposed (Nguyen et al., 1998) K^+-dependent release cycle leads to parallel, not antiparallel, local calcium oscillations. Interestingly, we find that local calcium oscillations observed on a seconds scale in permeabilized cells might be driven by the slow inactivation of channels organized in discrete clusters composed of between 6 and 15 channels, and out-of-phase calcium variations appear at rather constant luminal K^+. Contrary to the expectation, active implication of K^+ actually appears as a key factor in inducing parallel oscillations.

INTRALUMINAL CALCIUM DYNAMICS

In the following we consider the observation (Nguyen et al., 1998) that the glycoprotein matrix inside calcium stores functions as a continuous Ca^{2+}/K^+ exchanger. We have used a simple model for describing this commerce, whereby Ca^{2+} and K^+ compete in binding to a common matrix domain M, as shown in Fig. 1. Ion binding kinetics is assumed to be first-order for calcium and h_K-order for potassium. All over the paper h denotes Hill coefficients; k, rate constants, K, apparent dissociation constants, and $[X]$, concentration of the X specie. Then the equations governing the dynamical changes in the luminal concentrations read:

$$\frac{d[MCa]}{dt} = k^{on}_{MCa} \times [Ca^{2+}]_{lum} \times [M] - k^{off}_{MCa} \times [MCa] \quad (1)$$

$$\frac{d[MK]}{dt} = k^{on}_{MK} \times [K^+]^{h_k}_{lum} \times [M] - k^{off}_{MK} \times [MK] \quad (2)$$

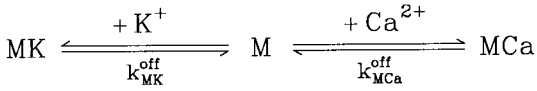

FIGURE 1 Reactions assumed in Ca^{2+} and K^+ competing binding to the same luminal matrix domain M.

$$\frac{d[Ca^{2+}]_{lum}}{dt} = -\frac{d[MCa]}{dt} \quad (3)$$

$$\frac{d[K^+]_{lum}}{dt} = -h_K \times \frac{d[MK]}{dt}, \quad (4)$$

where $[M] + [MCa] + [MK] = M_{max}$ is the total common Ca^{2+}/K^+ binding domains concentration.

Assuming that all luminal calcium in resting cells does not leak from the store during the experimental procedure (Nguyen et al., 1998) with blockage of IP_3Rs (by heparin) and of Ca^{2+}-ATPase (in absence of ATP), the stationary state of the system obtained when clamping the intraluminal $[K^+]$ (with nigericin) is readily obtained as:

$$[Ca^{2+}]_{lum} + \frac{[Ca^{2+}]_{lum} \times M_{max}}{K^{lum}_{Ca} \times \left[1 + \frac{[Ca^{2+}]_{lum}}{K^{lum}_{Ca}} + \left(\frac{[K^+]_{lum}}{K^{lum}_{K}}\right)^{h_K}\right]} = [Ca]^{rest}_{lum}, \quad (5)$$

where $[Ca]^{rest}_{lum} = [Ca^{2+}]^{rest}_{lum} + [MCa]^{rest}$ is the total luminal calcium (free + bound) content of resting (unstimulated) permeabilized cells in 140 mM K^+ incubating medium. Here the apparent dissociation constants are defined as $K^{lum}_{Ca} = k^{off}_{MCa}/k^{on}_{MCa}$ and $K^{lum}_{K} = (k^{off}_{MK}/k^{on}_{MK})^{1/h_K}$.

The best fit (shown in Fig. 2) of the data (Nguyen et al., 1998) to Eq. 5 was obtained with the following parameter values:

1). For the endoplasmic reticulum: $K^{ER}_{Ca} = 567.241\,\mu M$, $K^{ER}_{K} = 96.207\,mM$, $M_{max} = 3879.31\,mM$, $[Ca]^{rest}_{ER} = 362.069\,mM$ and $h_K = 6.276$; and

2). For isolated secretory vesicles: $K^{G}_{Ca} = 101.579\,\mu M$, $K^{G}_{K} = 79.473\,mM$, $M_{max} = 250\,\mu M$, $[Ca]^{rest}_{G} = 31.052\,\mu M$, and $h_K = 10.87$.

The obtained constant of Ca^{2+} dissociation from the ER protein matrix comes in agreement with generally accepted K^{ER}_{Ca} values. However, the model suggests the existence of a huge Ca^{2+} binding sites pool in the ER, of which the major part is masked by K^+, and Ca^{2+} appears to compete with six

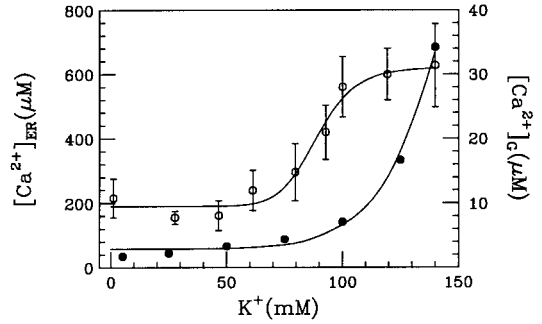

FIGURE 2 Derivation of intraluminal Ca^{2+}-K^+ exchange parameters. Fit of data (Nguyen et al., 1998) to Eq. 5 is obtained by least-square method. Either plot (Ca^{2+}_{ER}, *filled circles*, or Ca^{2+}_{G}, *open circles*) is drawn by using the corresponding parameters specified in the text.

K^+ ions inside the endoplasmic reticulum of cilliated cell or with 11 K^+ ions inside the mucin granules of goblet cells. To the moment there is no proof for such high cooperativity. Obviously, a better analysis would be possible if other data were available, so the model remains open to improvement. Let us see now how it does integrate with the present experimental evidence.

Regulation of the steady free calcium level (100 μM−300 mM) inside the ER is thought to be achieved through binding of Ca^{2+} ions to luminal glycoproteins as calsequestrin or calreticulin (Nguyen et al., 1998). Purified calsequestrin (with 109 acidic amino acids) binds ~40 mol Ca^{2+}/mol of calsequestrin with $K_D = 0.4-1$ mM at 150 mM KCl (Mitchell et al., 1988), and 1 mol of calreticulin binds ~20 mol Ca^{2+}. A quick inspection of our results shows that a mean buffer protein concentration of ~360 mM/40 ~ 10 mM would rely inside the ER of cilliated cells. Biochemical analysis should reveal the value of M_{max} in the absence of K^+. In favor of this, a decrease in the K^+ concentration from 150 mM to 20 mM was shown to induce a 6- to 10-fold increase in Ca^{2+} binding, meaning that a single protein molecule can bind ~400 Ca^{2+} ions at 20 mM K^+, thus supplying a large number of Ca^{2+} binding sites of the order 400×10 mM = 4 M. The 6- to 10-fold increase in calcium binding also agrees with our result $M_{max}/[MCa]^{rest} \simeq 10$.

In the mucin granules of goblet cells, the resting Ca^{2+} level is ~20 μM (Nguyen et al., 1998). The same calculation as above yields a quantity of ~500 nM luminal binding protein. The different K_{Ca} and h_K obtained with the two organelles suggest differences in intraluminal conditions (pH, chemical composition, or homogeneity degree) between different calcium stores. Nevertheless further diversity may be due to the cell type (cardiac/cilliated/goblet) or environmental (in vitro/in vivo) conditions (pH, ionic strength) of analysis. This, and the small amount of data, could explain why such a large capacity of intraluminal proteins to bind Ca^{2+} has not been detected yet. Quantitative measure of the K^+ binding capacity of ER buffers would be extremely valuable in determining the exact mechanisms involved in the luminal Ca^{2+}/K^+ ion exchange.

Two other points are to be stressed here. One, it is possible that at very low calcium concentration, the ER membrane gets very leaky, similarly to the plasma membrane (Hille, 1992), so we preferred removing the low calcium data, which otherwise alter the fit. Second, the above parameters constrain a minimal free resting $[Ca^{2+}]_{ER}^{rest} = 58.29\,\mu$M, which seems to disagree with the 25−35 μM values observed (Nguyen et al., 1998). We distinguish between two possible explanations for this apparent discrepancy. First, the data on steady-state Ca^{2+}/K^+ ion exchange in both the ER and secretory vesicles are obtained with pH 5.5, whereas $pH_{ER} = 7.1$ has been determined in vivo in HeLa cells (Kim et al., 1998). The most reasonable assumption is that a higher, physiological pH might change the Ca^{2+} and K^+ affinities for the luminal matrix. Indeed, a steady $[Ca^{2+}]_{ER}^{rest} =$ 25−35 μM can be readily obtained with calculation based on the assumption that K_{Ca}^{ER} and K_K^{ER} are reduced by the increased pH through a factor $f_{dis} > 1$ (discussed later on). As a second possibility, we assume $f_{dis} = 1$ (the pH has no effect on K_{Ca}^{ER} and K_K^{ER}) and consider calcium outflow at rest. Inasmuch as a steady state is reached in the Ca^{2+}/K^+ exchange experiments, we infer that the corresponding flux is flowing through the IP_3Rs; otherwise the lumen eventually gets empty. This scenario works if IP_3Rs have nonzero open probability in resting cells, which implies a basal, endogenous $[IP_3] > 0$. In the absence of any other data that could clarify these aspects, we shall consider both alternatives in our simulations on calcium release.

MODEL FOR FAST GATING OF THE IP_3R/Ca^{2+} CHANNEL

IP_3 binds to a specific protein complex—the IP_3R/Ca^{2+} channel, located on intracellular Ca^{2+} stores where it promotes and regulates release of Ca^{2+} into the cytosol. Each IP_3R is a tetramer having a well-defined IP_3 binding site per subunit ($K_d \simeq 50$ nM) near its NH_2-terminus (Marshall and Taylor, 1993; Taylor and Traynor, 1995). Two additional sites, with low ($K_d \simeq 10\,\mu$M) and high ($K_d \simeq 1$ nM) Ca^{2+} affinity have been described (Kaftan et al., 1997; Moraru et al., 1999), but their location is uncertain. Among all IP_3 binding sites, the 1-nM site is the least (≤1%) frequent.

Biochemical studies indicated that Ca^{2+} binds to the same receptor at up to eight sites per monomer (Mignery et al., 1992; Sienaert et al., 1996, 1997), with seven sites residing on the cytosolic region of the receptor (Sienaert et al., 1997). The Ca^{2+} affinity has been determined for only one of these sites (K_d = 0.8 μM, Hill coefficient 1). The luminal Ca^{2+} binding site (Sienaert et al., 1996) could modulate the channel activity as in the case of the homologous Ca^{2+} release channel of skeletal and cardiac muscle, the RyR, where the existence of such site has clearly been evidenced (Györke and Györke, 1998). The IP_3R is currently considered to be regulated by two functional classes of cytosolic calcium binding sites, of which one is activating (we denote it S_a) and one inhibitory (S_i). With the channel in its ER membrane environment, the open probability (P_o) data in the presence of 10 μM IP_3 are well described by a biphasic Hill formula (see Eq. 1 in Mak et al., 1998), whereby Ca^{2+} binds to S_a with activation constant $K_a = 210 \pm 20$ nM and Hill coefficient $h_a = 1.9 \pm 0.3$, and to S_i with $K_i = 54 \pm 3\,\mu$M and Hill coefficient $h_a = 3.9 \pm 0.7$. As for bilayer experiments, with 2 μM IP_3 applied, the channel's activity is maximal in the presence of 0.25 μM cytosolic Ca^{2+} (Bezprozvanny et al., 1991; Kaftan et al., 1997) and completely inhibited at 5 μM Ca^{2+}, showing both positive and negative feedback of Ca^{2+} in a bell-shaped $P_o([Ca^{2+}])$ curve, whereas with 180 μM IP_3 there is maximal activity at 1 μM Ca^{2+}, with a shallow decline at Ca^{2+} up to 40 μM. The predictions here (Bezprozvanny et al., 1991; Kaftan et al., 1997) for the K_d's are in the range 0.03−0.2 μM for the activating site and 0.2−1 μM for the inhibitory site, with two or three Ca^{2+} ions required to bind to the channel for each class of sites.

The regulatory domain of the receptor also includes two−three putative adenine nucleotide-binding sites (Marshall and Taylor, 1993; Taylor and Traynor, 1995). ATP bound to these sites stimulates the receptor, but the way it does so has to be clarified. Direct and systematic investigations (Mak et al., 1999) of the mechanism involved in this regulation showed that ATP allosterically regulates the Ca^{2+} sensitivity of the Ca^{2+} activating sites with a functional dissociation constant $K_{ATP} = 0.27$ mM and Hill coefficient of 1, meaning that only one ATP molecule binds to the receptor to stimulate it. The same study suggest that ATP is also involved in the regulation of the Ca^{2+} affinity of the inhibitory sites, but the data are not sufficient to draw a firm conclusion.

The type I IP_3 receptor has been shown to have a high open probability, $P_{o,max} \simeq 0.81$ (Mak et al., 1998, 1999), in its native membrane environment,

at the physiologic IP_3 ($\sim$1 μM) and cytosolic Ca^{2+} concentration ($[Ca^{2+}]_{cyt}$ $\sim$0.1 μM), although displaying a greatly reduced activity when incorporated into lipid bilayers, $P_{o,max} \simeq 0.04$ (Kaftan et al.,1997), respectively. In either case the P_o dependence on calcium (Bezprozvanny et al., 1991) is bell-shaped, as has been shown also for IP_3-induced calcium-45 release in brain synaptosoms (Finch et al., 1991). The data used and analyzed so far in various theoretical models are those obtained with the channel incorporated in artificial membranes. To describe its activity, 8- (De Young and Keizer, 1992), 16- (Kaftan et al., 1997), 18- (Swillens et al., 1999) and recently more complex, 125-state (Moraru et al., 1999) models have been proposed, out of which only the last one describes features of both P_o and open-time distributions.

Here we use and analyze data exclusively obtained with channels in their native environment and construct a simple operational model to accurately describe not only P_o but also τ_o (open time) and τ_c (close time), which is quite a difficult task. Our first steps were to consider first a two-site (four-state) and then three-site (eight-state) model. However, the quantitative results were unsatisfactory, for the models in no way could simultaneously fit the three data sets (Mak et al., 1998). We then added a fourth regulatory site and obtained good agreement to the data.

So, our minimal model treats the tetramer receptor as a complex unit, equivalent to a 16-state system at thermal equilibrium. Kinetics of calcium binding at either site are independent of each other, but dependent on binding to the receptor of a specific factor, f_a or f_i, respectively, as shown in Fig. 3 *A*. Hence, we are introducing two other regulatory sites, S_{fa} and S_{fi}. Because the open dwell time histograms of this channel generally show two distinct components, we assume there are two open states, characterized by bound S_a and both S_i and S_{fi} unbound.

Consequently, our model considers two main independent gating components, described by a reaction scheme of the form depicted in Fig. 3 *A*. From a structural point of view, each gating module represents a channel domain that includes two regulatory sites: S_a, S_{fa} for the activating gate, and S_i, S_{fi} for the inhibiting gate. The steady-state open channel probability P_o can be easily derived (as shown in Appendix 1) by considering first-order kinetics for the (un)binding reactions, mass balance equations, and the thermodynamical equilibrium constraints (Hille, 1992)

$$K_{fx}^{eq} \times K_{x0}^{eq} = K_{fx0}^{eq} \times K_{x}^{eq}, \tag{6}$$

where $K_{(f)x}^{eq} = k_{(f)x}^{off}/k_{(f)x}^{on}$ ($x = a, i$) is the equilibrium constant of the transition $q_{(f)x} = 0$ to $q_{(f)x} = 1$. Here $q_{(f)x}$ is the site $S_{(f)x}$ occupancy (0 or 1) and $k_x^{on} = k_x^{off} \cdot ([Ca^{2+}]_{cyt}/K_x)^{h_x}$.

Based on estimation (see Appendix 2) of errors introduced by events undetected during recording of single-channel activity, the data obtained with the *Xenopus* oocyte type I IP_3R/calcium channel in patches of the outer nuclear membrane are well (least-square method) fitted with the parameter values given in Table 1, with arbitrary k_{fa}^{off}, k_{fa0}^{off}, and k_{fi}^{off}. Mean values of the parameters are obtained by best fit with $\tau_d = 0.3$ ms, the approximate experimental value (Mak et al., 1998; Mak, personal communication). Parameter deviations from mean values are determined such that theoretical curves obtained with 0.2 ms $\leq \tau_d \leq$ 0.4 ms remain within experimental error bars. The model simultaneously comes in good agreement (shown in Figs. 4 and 5) with the measured open/close time and P_o for the specific conditions of the electrophysiological experiments (Mak et al., 1998), namely: 1.5-μM *trans* Ca^{2+}, 10-μM IP_3, and 500-μM ATP on the cytosolic IP_3R side. We have to mention that we obtained a good agreement with the triplet data, i.e., τ_o^*, τ_c^*, and P_o^*, only when a high affinity calcium binding site ($K_a = 12$ nM) was afforded for. The 500-μM ATP data could be fitted as well with $K_{a0} =$ 0.3 μM and $h_{a0} = 2$, with essentially the same results.

However, the extreme case ($K_a = 12$ nM and $K_{a0} = 0.55$ μM) offers a more realistic view on channel gating mechanisms, as it can be directly correlated to the stimulatory effect of free ATP on activation of the IP_3R by cytosolic calcium. As one can note, the two Ca^{2+} dissociation constants discussed here are about the same as the activating constants (17 $\pm$ 3 nM and 480 $\pm$ 20 nM) obtained (Mak et al., 1999) at high and zero ATP, respectively. The interpretation of the allosteric factor f_a as free ATP can account for many of the features of ATP dependence of channel activity. So, binding of free ATP at the cytosolic site of the channel can be characterized by a Hill coefficient $h_{ATP} = 1.3 \pm 0.1$, and dissociation constant $K_{ATP} = 215$ $\pm$ 15 μM in the presence and $K_{ATP0} = 90 \pm 30$ mM in the absence of cytosolic calcium, yielding good theoretical fit (shown in Fig. 5) to the activation data of Mak at different ATP concentrations. Our interpretation is that Ca^{2+} has either a high or a 50 times lower affinity for its activating cytosolic site S_a, depending on whether free ATP is bound to the regulatory site S_{fa} or not. ATP binding to IP_3R shifts K_a to its low value and thus facilitates channel activation. With $K_{i0} = 18$ μM, the model yields also good agreement (not shown) to the τ_o and τ_c data (Mak et al., 1999) obtained with 0$-$12 μM ATP.

Our calculation (not shown) based on the procedure described (Appendices 1 and 2) proves that simpler gating models (with two or three regulatory sites) cannot adequately fit into the experimental data. We want to stress that the two gating modules discussed here have been developed from the two standard calcium sites. The hypothesis is made that kinetics of Ca^{2+} binding at each of these two sites are regulated by a distinct factor. At first we had devoted a lot of work to the identification of the ligand f_a as IP_3 but this resulted (not shown) in a marked dependence of the activation domain of the $P_o([Ca^{2+}]_{cyt})$ curve on the concentration of IP_3, contrary to the data (Mak et al., 1998). Another good candidate, namely ATP, for the same factor f_a has been suggested before (Mak et al., 1999) and we have proved here that interpreting ATP as the factor implicated in the activation module regulation very well can explain the related features of channel activity.

As for the inhibiting module, evidence is less conclusive. A good choice initially seemed to be IP_3, as in the model of De Young and Keizer (1992), with the IP_3 binding transition adapted to the present situation, but the results (not shown) came in disagreement with the IP_3 effects on P_o (Mak et al., 1998), mainly because $P_{o,max}$ greatly depended on IP_3 concentration, and the activation domain of the $P_o([Ca^{2+}]_{cyt})$ curve was shifted to the right by decreasing $[IP_3]$, which is not the case. Neither could ATP provide good explanation for this behavior (from our investigations, not shown). Consequently, we hypothesize here that the factor f_i might be luminal Ca^{2+}. In this way the model can explain key features of channel kinetical behavior, such as inhibitory effects of high (0.6$-$1 mM) $[Ca^{2+}]_{lum}$ in the absence of ATP (Thrower et al., 2000); apparent invariability of P_o at low $[Ca^{2+}]_{lum}$ (Mak et al., 1998); decreased open channel duration observed in the presence of calcium in the *trans* chamber (Bezprozvanny and Erlich, 1994); or the shallow decrease (Thrower et al., 2000) of the longest open time (here τ_{o1}) with increasing $[Ca^{2+}]_{lum}$. The implicated mechanism considered here is closing of the IP_3R by luminal Ca^{2+}, whereas for the RyR the opposite effect, namely opening of the luminal gate by calcium, can account for the data obtained (Györke and Györke, 1998). More precisely, for the IP_3R, the transition from the (0,0) to the (0,1) state of the inhibition module is assumed to be driven by calcium binding to the luminal site, thus

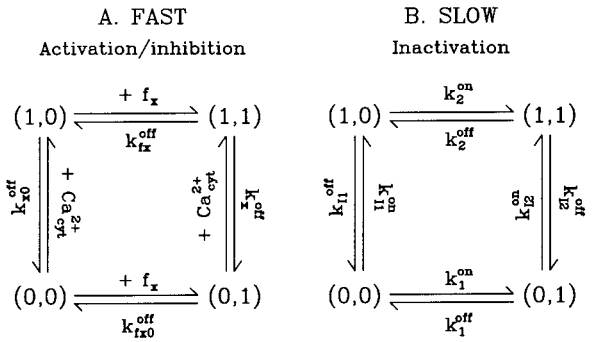

FIGURE 3 Four-state channel representation and transitions within basic regulatory modules of IP_3R fast and slow gating, as assumed in the model. In *A*, $x = a$ or i and $X = A$ or I characterize the activating and inhibitory module, respectively.

TABLE 1 Parameters of the fast-gating kinetics of the IP_3R

Gating process	Specific conditions	Parameter symbol	Description	Value
Ca^{2+} binding to its cytosolic activating site S_a	f_a unbound to S_{fa}	k_{a0}^{off}	Off-rate constant	$65 \pm 35\ s^{-1}$
		K_{a0}	Dissociation constant	550 ± 20 nM
		h_{a0}	Hill coefficient	1.8 ± 0.1
	f_a bound to S_{fa}	k_a^{off}	Off-rate constant	$270 \pm 70\ s^{-1}$
		K_a	Dissociation constant	12 nM
		h_a	Hill coefficient	2.1 ± 0.1
f_a binding to S_{fa}	Ca^{2+} bound to S_a	$\frac{k_{fa}^{on}}{k_{fa}^{off}}$	On-rate constant to off-rate constant ratio	3
Ca^{2+} binding to its cytosolic inhibitory site S_i	f_i unbound to S_{fi}	k_{i0}^{off}	Off-rate constant	$40 \pm 15\ s^{-1}$
		K_{i0}	Dissociation constant	$45 \pm 1\ \mu M$
		h_{i0}	Hill coefficient	3.2
	f_i bound to S_{fi}	k_i^{off}	Off-rate constant	$3 \pm 2.5\ s^{-1}$
		K_i	Dissociation constant	$18\ \mu M$
		h_i	Hill coefficient	3.2
f_i binding to S_{fi}	Ca^{2+} bound to S_i	k_{fi0}^{on}	On-rate constant	$210 \pm 30\ s^{-1}$
		$\frac{k_{fi0}^{off}}{k_{fi0}^{on}}$	Off-rate constant to on-rate constant ratio	4.5 ± 0.25

closing the channel (if open). It is quite difficult to make an exact correspondence between data obtained in different experimental conditions. Channel inactivation by 0.6−1 mM $[Ca^{2+}]_{lum}$ in absence of ATP agrees well with $h_{Ca}^{lum} = 0.3 - 0.4$ (our model predicts—not shown—that this inactivation is only apparent, with all open channel events being too short for detection with 0.5-ms time resolution (Thrower et al., 2000); in addition, removal of 1 mM $[Ca^{2+}]_{lum}$ inhibition by ATP would agree with an increase of K_{Ca}^{lum} with ATP, which pushes τ_o above the detection limit). Instead, for specific experimental conditions (Mak and Foskett, 1997), the value $h_{Ca}^{lum} = 0.9 \pm 0.1$ gives $\tau_{o1} \simeq 14-21$ ms and $\tau_{o2} \simeq 2-5$ ms values, close to those obtained by experiment ($\simeq 20$ ms and <5 ms, respectively), but implies a lower threshold for the inhibitory $[Ca^{2+}]_{lum}$ (~50 μM). The calculated subunitary Hill coefficient could result from negative cooperativity in calcium binding at the luminal site. It yields a dissociation constant $K_{Ca}^{lum} \simeq 6\ \mu M$ for $h_{Ca}^{lum} = 1$, and $K_{Ca}^{lum} \simeq 270\ \mu M$ for $h_{Ca}^{lum} = 0.3$.

The analysis here does not uniquely declare Ca_{lum}^{2+} as the factor f_i, but provides a series of arguments in favor of this equivalence. In further simulations we shall consider three possible alternatives on this matter (see below). As a final point here, it is worth mentioning that the IP_3 dependence of the $P_o([Ca^{2+}]_{cyt})$ curve can be well reproduced (not shown) by considering the proposed allosteric regulation of the calcium affinity for the S_i site by IP_3 binding to its 50-nM site with a Hill coefficient of 4 (see Eq. 2,

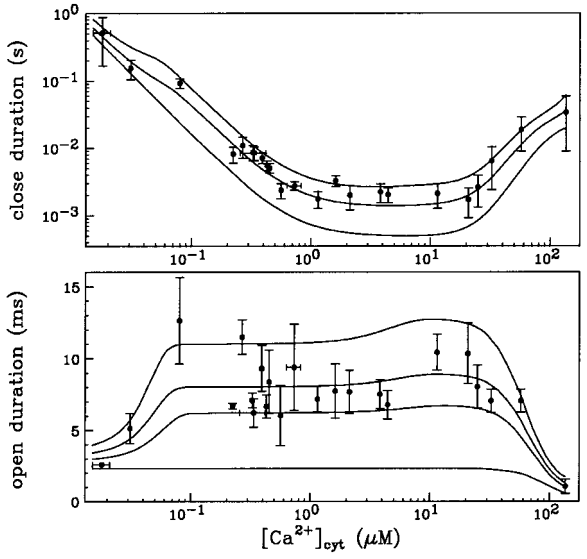

FIGURE 4 $[Ca^{2+}]_{cyt}$ dependence of the mean open- and closed-channel duration at 10 μM IP_3 and 500 μM free ATP. Data are from Mak et al. (1998) and Mak (personal communication). Continuous lines are drawn according to Eqs. 17−19 with parameter values given in the text. The curves in each panel correspond respectively, from the lowest to the upper, to different values of τ_d: 0, 0.2, 0.3, and 0.4 ms in the lower panel and 0, 0.2, and 0.4 ms in the upper panel.

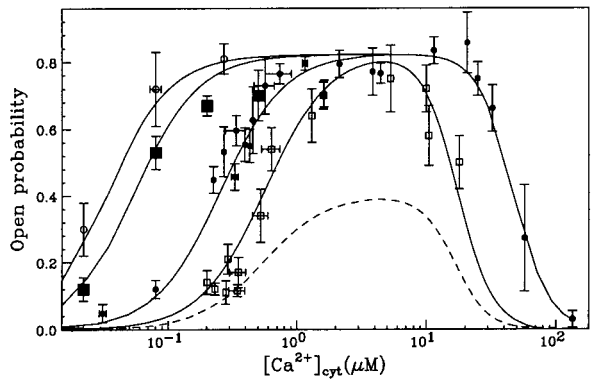

FIGURE 5 Open probability of IP_3R at 10 μM IP_3 and different cytosolic ATP concentrations: 0−12 μM (*small squares*), 500 μM (*filled circles*), 4.8 mM (*large squares*), and 9.5 mM (*open circles*). Data are from Mak et al. (1998, 1999). Curves represent calculated P_o^*. Actual P_o differs by <5% (not shown). Dashed line corresponds to predicted P_o at 1 mM $[Ca^{2+}]_{lum}$ in the absence of ATP, assuming $h_{Ca}^{lum} = 0.3$.

Mak et al., 1998), where $K_{max} = 54\ \mu M$ is replaced by the 45 μM obtained here. This dependence will be used in all our simulations (see below).

SIMULATION OF CALCIUM SIGNALS IN PERMEABILIZED CELLS

Because the calcium release apparatus seems to behave differently in various cell types, generating different patterns of Ca^{2+} signals, a better understanding of the molecular and cellular mechanisms involved is of great interest. Given the large differences between the channel's properties considered here as compared to previous theoretical studies, we have been looking for defining their effects and determining how the 16-state model could integrate into an operational model of calcium release. We expected largely different features of release kinetics because the channel is inhibited now at higher $[Ca^{2+}]_{cyt}$ ($\sim$100 μM vs. $\sim$1 μM). Furthermore, calcium release regulation by K^+ appears to be crucial in the oscillatory Ca^{2+} response to agonist stimulation, inasmuch as the calcium signal disappears (Nguyen et al., 1998) in the presence of apamin, a blocker of the small conductance calcium-activated potassium (ASK) channels (see below).

To quantitatively study the effects of potassium ions in calcium release regulation, we coupled the IP_3 gating model analyzed above to the dynamics of calcium and potassium in both the lumen and cytosol. Numerical and biophysical aspects of our simulation procedure are detailed in the Appendix 3. The model was tested first on a documented scenario (Nguyen et al., 1998) and improved to come in agreement with two basic processes: 1); calcium oscillations are triggered locally in permeabilized cells; and 2), K^+ is implicated in the (in- or out-of-phase) character of these oscillations. It is worth mentioning that a rise of such oscillations in permeabilized cells has not been theoretically explained yet. We have examined the system's behavior under various physiological constraints and inspected the sensitivity of the calcium signals to several parameters. To remain in agreement with the experimental evidence, further improvement of the model has emerged and critical ranges of the free parameters in the model have been determined.

Slow kinetics of calcium release

Simulations based on the 16-state model

At first we strictly used the scenario proposed (Nguyen et al., 1998) and considered (Scenario I) that the equilibrium resting state has low ($\sim$25$-$35 μM) $[Ca^{2+}]_{ER}$. Accordingly, we had to consider a potassium extrusion term, which could be due to the K^+-H^+ exchanger across the reticulum membrane (Nguyen et al., 1998), to restore the chemical equilibrium (see Eq. 5) inside the store. As mentioned before, we were led to lower the dissociation constants K_K^{ER} and K_{Ca}^{ER} by a factor f_{dis}. After IP_3 stimulation, the IP_3R/calcium channels open and the resulting increase in $[Ca^{2+}]_{cyt}$ activates the ASK channels on the ER membrane (Nguyen et al., 1998). Consequently, K^+ inflow liberates Ca^{2+} from the luminal matrix. In all our simulations, the system first displayed a pronounced but transient increase in local $[Ca^{2+}]_{cyt}$ ($\sim$3 μM) and ran thereafter into a quasi steady state with high $[Ca^{2+}]_{ER}$ (between 2 and 5 mM) and slightly elevated $[Ca^{2+}]_{cyt}$ ($\sim$0.6 μM). Calcium release is silenced by the inhibitory effect of the high microdomain (Naraghi and Neher, 1997) calcium concentration built up by a current as high as 0.4$-$1 pA flowing through the channel from the submembrane $[Ca^{2+}]_{ER}$ of $\sim$2$-$5 mM.

We then undertook the possibility that gating kinetics is modified in vivo (Mak and Foskett, 1997), and assumed 100 times slower channel gating. An example, obtained with $N_{Ca} = 2$, is shown in Fig. 6 *A*. Increasing N_{Ca} produces a similar first spike, followed by more frequent, smaller spikes. However, in all the cases we have investigated (for large variation of the free parameters (not shown)), the resulting variations in intra- and extraluminal free calcium concentrations were not out of phase as expected, but always parallel. In addition, these variations are irregular, not oscillatory-type.

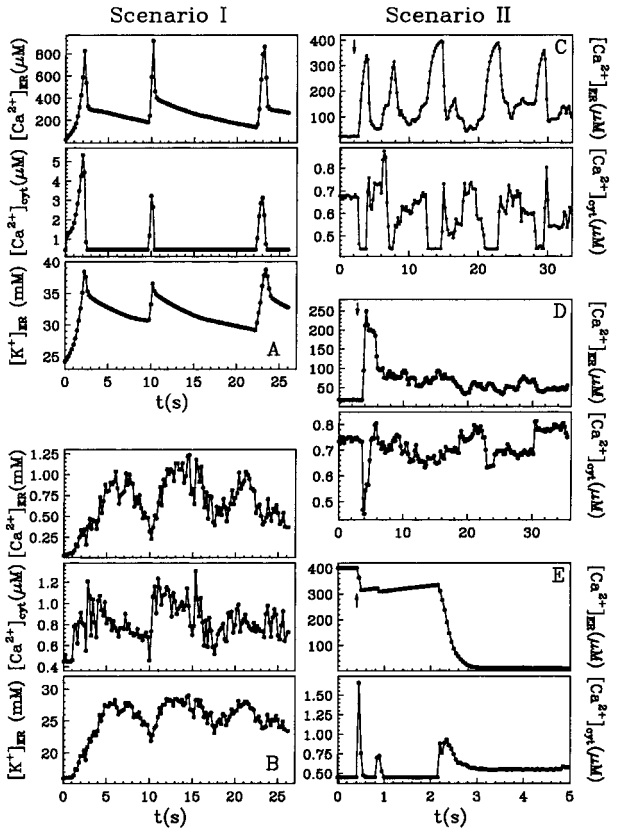

FIGURE 6 Simulated responses after stimulation of permeabilized cells with 3 μM IP_3 at $t = 0$ in *A* and *B* and at moments indicated by arrows in *C*, *D*, and *E*. In *C* and *D*, a basal $[IP_3]_b = 30$ nM and 100 μM EGTA are considered; otherwise EGTA is present with 40 μM.

Therefore, we have approached another strategy (Scenario II): we assumed that with all IP_3Rs closed, the store at equilibrium has $[Ca^{2+}]^0_{ER} \geq 350\,\mu M$ with a calculated $[K^+]^0_{ER} \geq 124.33\,mM$, assuming $f_{dis} = 1$. Then, we considered a basal $[IP_3]_b = 30$ nM, which drove $[Ca^{2+}]_{ER}$ to the rest value. However, within large parameter ranges, increasing IP_3 to 3 μM has no effect (not shown), which was not unexpected, inasmuch as the Ca^{2+} channel current is too small and the IP_3R P_o remains high.

A slow gating component is required

From the results obtained so far, we conclude that the simple model for IP_3R gating is not sufficient to explain the observed patterns of calcium signals. So, we suspected that a slow kinetic component of the *Xenopus* oocyte IP_3R has not manifested in vitro (Mak et al., 1998), or was too slow to be detected (see the case of the RyR that adapts 100 times slower in vitro than in vivo (Sachs et al., 1995). Recordings of the type I IP_3R activity in its native environment show indeed that an additional, slow kinetic component is active in vivo. However, analysis of inactivation at the receptor level is rendered extremely difficult by its slow kinetics, which reduces the number of events below a reasonable limit appropriate for a standard statistical analysis. When analyzed in the ''on-nucleus'' configuration (Mak and Foskett, 1997), the channel preserved its fast kinetics features (discussed above), but displayed an additional, slow kinetic component.

All these, along with observations that Ca^{2+} and IP_3 inactivate IP_3R and IP_3-mediated calcium release on a seconds scale (Parker and Ivorra, 1990; Finch et al., 1991; Hajnóczky and Thomas, 1994; Oancea and Meyer, 1996), have determined us to introduce a Ca^{2+}- and IP_3-dependent slow regulatory module. The reaction scheme, shown in Fig. 3 *B*, was first proposed to explain adaptive behavior and can account for channel inactivation after ligand binding (Sachs et al., 1995). The current active substates in Fig. 3 *B* are (1,0) and (0,1), so the channel has now four open states, which may correspond to the four different subconductance states observed experimentally (Bezprozvanny et al., 1991, Mak and Foskett, 1997; Thrower et al., 2000). We have chosen the functional dependence $k^{on}_{I1} = k^{off}_{I1} \times ([Ca^{2+}]_{cyt}/K_I)^{h_I} \times IP_3/(IP_3 + K_{IP_3})$ consistent with the interpretation (Hajnóczky and Thomas, 1994) that IP_3 may aid Ca^{2+} to access its inhibitory site (here by fastening Ca^{2+}-binding kinetics), and with three other observations: 1), the initial release rate increases (Hajnóczky and Thomas, 1994) with IP_3 in the range 1.5–7.5 μM, so we assume that the IP_3 site involved is the low affinity one, i.e., $K_{IP_3} = 10\,\mu M$; 2), the channel recovers from inactivation after IP_3 removal *or* chelation of calcium in the presence of saturating IP_3 (Hajnóczky and Thomas, 1994); and 3), half-maximal channel inactivation appears at ~0.2 or 0.6 μM $[Ca^{2+}]_{cyt}$ (Finch et al., 1991; Hajnóczky and Thomas, 1994); we use then $K_I = 0.2$ μM and $h_I = 2$, as proposed for channels in reconstituted bilayers (Bezprozvanny et al., 1991). The thermodynamical condition was used as before to derive k^{on}_{I2}. Other parameters were chosen to yield two inactivation components that differ by at least one order (Hajnóczky and Thomas, 1994) and to match as possible the results of Mak and Foskett (1997). For the conditions therein (10 μM IP_3, 1 mM ATP, 200 nM $[Ca^{2+}]_{cyt}$, and 200 nM $[Ca^{2+}]_{lum}$), event distributions generated by the full 64-state model satisfactorily agree (not shown) with both P_o and the mean open and closed time histograms for two sets of kinetic parameters, as specified in Table 3. Analytical and simulated activity of the 64-state, but not 16-state, channel shows inactivation (not shown) of biexponential time course with rate constants of the order of those determined by experiment (Hajnóczky and Thomas, 1994).

Simulations based on the 64-state model

With the new code applied to Scenario II and using the Set 1 of parameters in Table 3, out-of-phase oscillations were obtained similar to those observed (Nguyen et al., 1998). A typical result is shown in Fig. 6 *C*. The Ca^{2+} response strongly depends on k^{off}_{MCa}. Sharp $[Ca^{2+}]_{ER}$ variations were routinely obtained with $k^{off}_{MCa} = (1.2 \pm 0.5) \times 10^{-3}\,s^{-1}$. Higher k^{off}_{MCa} induce rapid Ca^{2+} mobilization and $[Ca^{2+}]_{ER}$ remains high. Slow Ca^{2+} dissociation induces rapid store depletion and return of $[Ca^{2+}]_{cyt}$ to a near-basal level after a transient increase (Fig. 6 *E*, obtained with $N_{Ca} = 6$ and $k^{off}_{MCa} = 3 \times 10^{-4}\,s^{-1}$). Another determining factor shaping the calcium response has been found as the receptor density (Swillens et al., 1999). At low density ($N_{Ca} < 9$), the nonconducting channel periods are generally longer and become highly irregular as $N_{Ca} \rightarrow 1$. We typically obtained oscillatory-like behavior with $N_{Ca} = 9-12$ (the simulation in Fig. 6 *C* was obtained with 12 channels per cluster and 1.3 μm lateral spacing between clusters). Increasing N_{Ca} reduces the chance that all channels in the cluster are not simultaneously conducting and the interval between inactivity periods becomes longer. In three simulations with $N_{Ca} = 25$ (one shown in Fig. 6 *D*), we did not obtain a second complete cluster inactivation within 40 s.

Because the present data on the dependence of IP_3R gating on luminal calcium are not conclusive, we relaxed the assumption (see above) that $f_i \equiv Ca^{2+}_{lum}$ by considering either a weak dependence ($h^{lum}_{Ca} = 0.3$) or independence (i.e., $k^{on}_{fi} =$ constant) of the inhibitory module on Ca^{2+}_{lum}. Both choices were not critical to the results. On the contrary, in several simulations (not shown) with the same conditions but $h^{lum}_{Ca} = 1$, the channels' P_o decreases considerably at $[Ca^{2+}_{lum}] \geq 350\,\mu M$ so that the system remained in a quasi steady state with high Ca^{2+}_{lum} and low Ca^{2+}_{cyt}. We have not followed this line of investigation, inasmuch as it would be only speculative at the moment. In numerous simulations we have varied the EGTA concentration as specified in Table 2, but its effect on the slow timescale was not critical, as it

TABLE 2 Standard parameters in calcium release simulations

Symbol	Description	Value	References/comments
r_T	ER tubule radius	190−300 nm	Limited by computational time
r_C	Cytosolic depth from the ER tubule membrane	2 μm	Swillens et al., 1998
z_T	Length of the ER tubule segment ≡ distance between two release sites	0.75−1.5 μm	Horne and Meyer, 1997; Callamaras and Parker, 1999
$B_{T,fix}$	Total concentration of the stationary buffer	120−300 μM	Clapham, 1995; Swillens et al., 1998; Haddock et al., 1999
$K_{B,fix}$	Dissociation constant of the stationary buffer	10 μM	Swillens et al., 1998
$k^{on}_{B,fix}$	On-rate constant of the stationary buffer	10^8 M^{-1} s^{-1}	Clapham, 1995
$B_{T,mob}$	Total concentration of the mobile buffer (EGTA)	40−100 μM	Relatively low level, to minimize the slowing down effects on calcium release (Horne and Meyer, 1997)
$K_{B,mob}$	Dissociation constant of the mobile buffer (EGTA)	170−670 nM	Pape et al., 1995; Naraghi and Neher, 1997
$k^{on}_{B,mob}$	On-rate constant of the mobile buffer (EGTA)	1.5−2.5 μM^{-1} s^{-1}	Pape et al., 1995; Naraghi and Neher, 1997
$[K^+]_{ext}$	Constant cytosolic $[K^+]$ at $r > r_C$	140 mM	Nguyen et al., 1998
$[Ca^{2+}]_{ext}$	Constant cytosolic $[Ca^{2+}]$ at $r > r_C$	450 nM	Nguyen et al., 1998
[ATP]	Constant cytosolic [ATP]	3 mM	Nguyen et al., 1998
$[IP_3]$	Constant cytosolic $[IP_3]$	3 μM	Nguyen et al., 1998
D^{cyt}_{Ca}	Diffusion coefficient of Ca^{2+} ions in the cytosol	200−220 μm^2 s^{-1}	Clapham, 1995; Naraghi and Neher, 1997
D^{ER}_{Ca}	Diffusion coefficient of Ca^{2+} ions in the lumen	20−50 μm^2 s^{-1}	Kargacin, 1994; Clapham, 1995. One order lower than D^{cyt}_{Ca}, to correct for buffers and extremely tortuous ion pathway
D^{cyt}_{K}	Diffusion coefficient of K^+ ions in the cytosol	1500−2000 μm^2 s^{-1}	Hille, 1992
D^{ER}_{K}	Diffusion coefficient of K^+ ions in the lumen	50−160 μm^2 s^{-1}	One order lower than D^{cyt}_{K}, as for Ca^{2+}
$D^{cyt}_{B,mob}$	Diffusion coefficient of EGTA in the cytosol	170−220 μm^2 s^{-1}	Pape et al., 1995; Naraghi and Neher, 1997
r^{cp}_{Ca}	Capture radius of the Ca^{2+} channel	4−12 nm	Chosen to yield a saturating Ca^{2+} current ≅0.1 pA at 500 μM $[Ca^{2+}]_{ER}$ (Bezprozvanny and Erlich, 1994; Swillens et al., 1998); corresponds roughly to the dimen sion of the square-shaped mouth of the channel (Swillens et al., 1998)
r^{cp}_{K}	Capture radius of the K^+ channel	0.3−4 nm	Hille, 1992
g_{Ca}	Single-channel conductance of the Ca^{2+} channel	113 pS	Mak and Foskett, 1997
g_K	Single-channel conductance of the K^+ channel	15−20 pS	Vergara et al., 1998
K_P	Smooth ER Ca^{2+} pump's activation constant	0.1−1 μM	De Young and Keizer, 1992; Dupont and Goldbeter, 1994
T	Temperature	298 K	

mainly operates on the signal's amplitude, which remains in the noninhibitory $[Ca^{2+}]_{cyt}$ domain (not shown).

Efficiency of interchannel communication was shown (Swillens et al., 1999) to decrease with the distance between receptors (d), and a compact (d = 12 nm) cluster of ~20−30 channels could explain the currently observed distributions of puffs and blips. Due to the high complexity of the system, our spatial grid was always $d \geq 35$ nm. As an alternative (Swillens et al., 1999) we also performed several simulations where a highly compact cluster of 25 channels was comprised in a unique volume element, with 50-nm gridding. The open probabilities were independently simulated for all channels, which are facing now the same microdomain $[Ca^{2+}]_{cyt}$. The results obtained with this procedure are not qualitatively different from those shown in Fig. 6 *D*.

TABLE 3 Parameters of slow-gating kinetics of the IP_3 receptor

	Value	
Symbol	Set 1*	Set 2†
k^{off}_{I1}	0.75 s^{-1}	0.075 s^{-1}
k^{off}_{I2}	0.075 s^{-1}	0.75 s^{-1}
k^{on}_{1}	0.25 s^{-1}	0.081 s^{-1}
k^{off}_{1}	0.175 s^{-1}	0.25 s^{-1}
k^{on}_{2}	0.5 s^{-1}	0.2 s^{-1}
k^{off}_{2}	0.05 s^{-1}	0.05 s^{-1}

*Active substates are (1,0) and (0,1) in Fig. 3 *B*.
†Active substates are (0,0) and (1,1) in Fig. 3 *B*.

Extremely high density of IP_3Rs corroborated by rapid Ca^{2+} mobilization inside the ER can produce sustained, high global $[Ca^{2+}]_{cyt}$ after stimulation, without requiring external calcium influx as currently invoked for explaining a high Ca^{2+} level in some cells after stimulation (Dupont, 1999). For example, a formation of six clusters, 50-nm interspaced, each consisting of 20, highly packed IP_3Rs, yields (not shown) an elevated *global* $[Ca^{2+}]_{cyt}$ fluctuating between 0.83 and 0.94 μM, whereas the radial average varies between 29−38 μM and $[Ca^{2+}]_{ER}$ remains at 100−113 μM, for $k^{off}_{MCa} = 4 \times 10^{-3}$ s^{-1}.

Use of the full model according to Scenario I generates parallel variations in local intra- and extraluminal calcium (an example is shown in Fig. 6 *B*, obtained with $N_{Ca} = 9$ and the Set 2 of inactivation parameters). Differences between simulations using either of the two sets of inactivation parameters were not crucial for the dynamical behavior of the system. We also have checked that with $K_I = 0.66$ or 0.8 μM (Finch et al., 1991; Moraru et al., 1999) and $h_I = 1$ or 2, oscillatory evolution can as well be reproduced within both scenarios, in conditions mentioned above.

From a careful inspection by simulation (not shown) we conclude that variation of the standard parameters within ranges given in Table 2 do not result in qualitative changes in the shape of calcium signals on the seconds timescale. Instead, the completely free parameters left (namely N_{Ca}, N_K, f_{dis}, k^{off}_{MCa}, and k^{off}_{MK}) appear to be crucial in their modulation. Generally we used $N_{Ca} = 1-25$ (Swillens et al., 1999) and $N_K = 50-250$. We have examined the system's response to large variations in these parameters (not shown). Depending on the scenario, Table 4 indicates parameter values constrained by the requirement to obtain realistic results. For example, within Scenario I, the values therein give fast Ca^{2+} mobilization and results relevant to the situation. Lower values greatly enlarge the dynamic profiles (not shown). In summary, the system's behavior was found to be extremely sensitive to three factors:

1. The rapidity of Ca^{2+} and K^+ ions in dissociating from the luminal glycoprotein matrix.
2. The number of Ca^{2+} channels in the cluster.
3. The difference between the luminal and cytosolic K^+ concentration.

Fast kinetics of calcium release

An example of stochastical simulation (based on the 64-state model of the IP_3R/Ca^{2+} channel gating) of subseconds calcium release at a single channel release site according to Scenario II is presented in Fig. 7. Here the luminal equilibrium is determined by the level of 400 μM $[Ca^{2+}]_{lum}$ and that of 127.5 mM $[K^+]_{lum}$ (calculated from Eq. 5). During short openings of the IP_3R, an initial current of ~0.1 pA rapidly (<1.5 μs) elevates the average calcium concentration to ~50 μM in the spatial element (denoted *1st* in Fig. 7 *B*) facing the cytosolic mouth of the channel. The 50-μM value comes in agreement with the calculated Ca^{2+} profile near (~50-nm distance) the mouth of the channel in a hemispherical space (Naraghi and Neher, 1997). A steady state is reached within ~160 μs by equilibration of store calcium outflow with cytosolic Ca^{2+} buffering, diffusion, and pumping back into the store, provided calcium stabilizes also in the luminal submembrane element (denoted *1st* in Fig. 7 *C*; this requirement can be met if k^{off}_{MCa} is not too low). At the plateau phase, the channel current is reduced to half-maximal value as a consequence of reduction in the local ER-cytosol Ca^{2+} gradient. Channel closure is followed by rapid dissipation in the cytosol, so that complete recovery follows channel shut within ~24 ms. During the whole period of calcium release and consequent dissipation through the cytosol, a corresponding local Ca^{2+} wave spreads over a maximal radial distance of ~1 μm (d_{max} in Fig. 7 *D*), with a total duration of ~24 ms. The resulting variations in local calcium concentrations are parallel on the ms scale of channel activity. Global $[Ca^{2+}]_{cyt}$ display a rapid rise immediately after channel opening and a biphasic decrease after channel closure (see Fig. 7 *D*) with decay constants of the order 1 ms and 40 ms, respectively. The rise phase duration is correlated with the channel open time and not with luminal calcium.

TABLE 4 Parameters used in simulations using Scenario I or II

Symbol	Description	Value	
		Scenario I	Scenario II
N_K	Number of ER K^+ channels	100–250	50–100
f_{dis}	Factor of increasing Ca^{2+} and K^+ affinity for the luminal matrix	5–8	1
k^{off}_{MCa}	Off-rate constant for dissociation of Ca^{2+} from the luminal matrix	10–50 s^{-1}	(0.3–3) × 10^{-3} s^{-1}
k^{off}_{MK}	Off-rate constant for dissociation of K^+ from the luminal matrix	10–50 s^{-1}	(3–100) × 10^{-3} s^{-1}

The corresponding pattern displayed by a multichannel release site is presented in Fig. 8, where the cluster comprises nine receptors 40-nm interspaced. Local concentrations are calculated with respect to the central channel, which in this simulation performs a single, short opening where the channel current comes to ~81 fA. As expected, the region (denoted *1st*) facing the cytosolic side of the central IP_3 receptor senses transient elevations (4–14 μM) induced by openings of channels. During sustained activity of the cluster, the free calcium concentration initially increases in the overall cytosolic volume, then (after ~50 ms) saturates during a relatively steady release and eventually decays (time constants as above) to the basal level at the end of longer (of the order 100 ms) nonconducting periods.

A second possibility for modulation of calcium release by luminal calcium corresponds to the mechanism proposed (Nguyen et al., 1998) (here Scenario I). In Fig. 9 we show the time course followed by calcium released from the ER with low equilibrium level: 30 μM $[Ca^{2+}]_{lum}$ and 16 mM $[K^+]_{lum}$, obtained with $f_{dis} = 7$. The calcium channel current is now lower than in the previous situation (see Figs. 7 and 8), but increases during release as the submembrane luminal calcium raises. The resulting variations in local luminal calcium and potassium are parallel, being driven by openings of the nearest potassium channel(s) that follow, on a longer timescale, the cytosolic colocalized Ca^{2+} accumulation. After the initial increase, the obtained cytosolic Ca^{2+} signal displays saturation again, followed by biphasic decay (time constants ~1 ms and ~40 ms) to the basal level within $\simeq$ 170 ms.

DISCUSSION

This study was motivated by the newly unveiled implication of K^+ ions in intraluminal calcium handling, and one of its

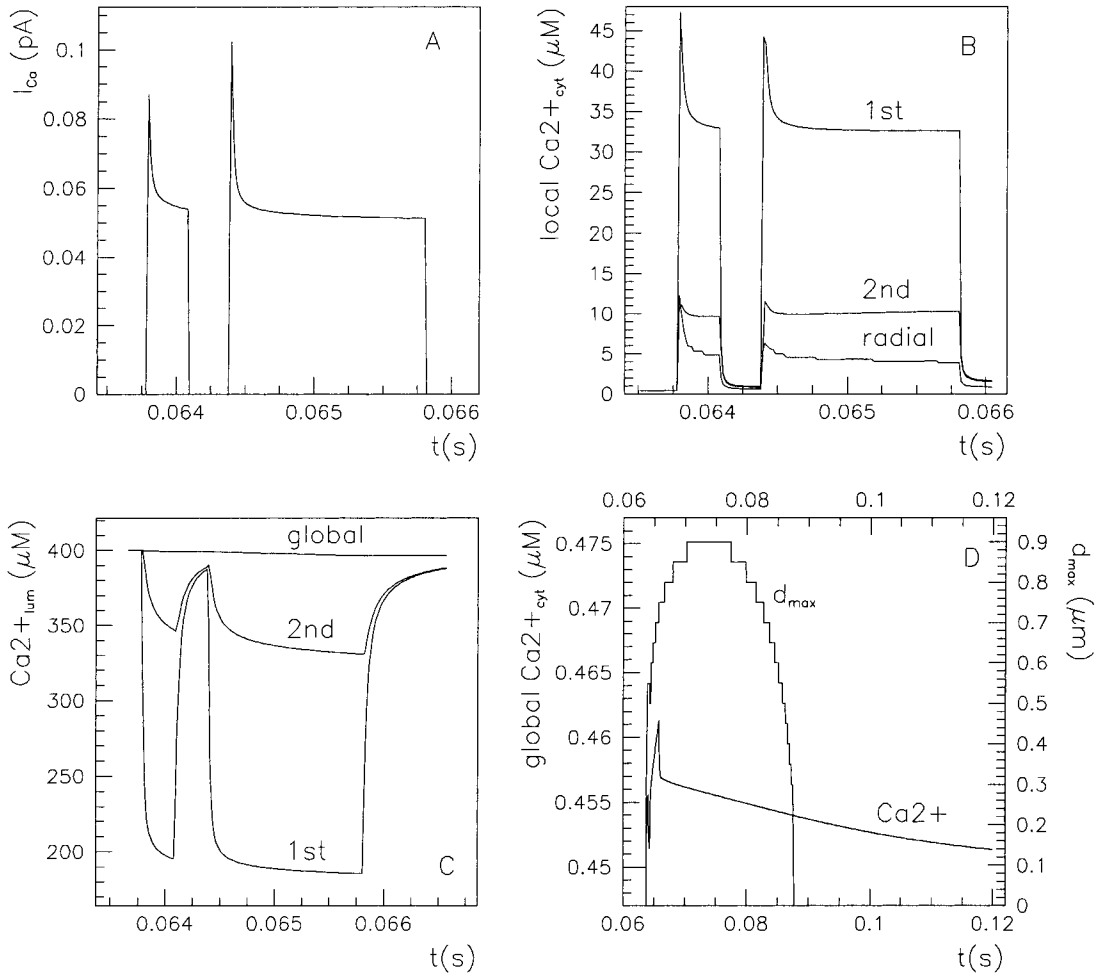

FIGURE 7 Subseconds calcium release at a single channel site, according to Scenario II. During the 120 s lapsed after 3 μM IP_3 stimulation, the channel displays two openings and the corresponding effects are visualized as evolutions of the ionic current (*A*), local cytosolic (*B*), or luminal (*C*) Ca^{2+} concentration, as well as the global cytosolic calcium signal and wave propagation within the cytosol (*D*). The buffering level is given by 200 μM endogenous fix buffer and 40 μM EGTA.

goals was to investigate its concrete effects on the complex process of calcium release from the ER. To this end we construct a simple model to describe the ER Ca^{2+} channel activity in its native membrane environment and approach various, realistic alternatives to obtain best fits to the data. It is inconveniently true that the high number of factors involved in the dynamic regulation of this channel activity as well as the limited data, which not rarely give rise to discrepancies, imprint a rather speculative character to any theoretical analysis of the calcium release process. However, even simple models that are able to explain most general features of the process have proved valuable tools in the study of the detailed mechanisms of intracellular calcium signaling.

Initially, most models (De Young and Keizer, 1992; Atri et al., 1993; Bezprozvanny and Erlich, 1994) considered three sites responsible for channel activity regulation: one site for IP_3 and two sites for Ca^{2+}, one activating and one inhibitory. Within this scheme, the IP_3 effect on P_o could partially be described by the De Young and Keizer model only. More recently, a low affinity IP_3 binding site was included (Kaftan et al., 1997) to explain how the $P_o([Ca^{2+}])$ curve is rightward-shifted by increasing IP_3 and inhibition by up to 50 μM Ca^{2+} relieved. Later, this model has been reformulated (Moraru et al., 1999) to give better fits to the P_o and τ_o data in dependence on both Ca^{2+} and IP_3. To this end, it was assumed that each receptor monomer contains one Ca^{2+} regulatory site and two IP_3 sites, of medium and low affinity, respectively. Another combination has been used in agreement to the P_o data at 2 μM IP_3 (Bezprozvanny et al., 1991), by considering one IP_3 site, two Ca^{2+} activating sites, and two Ca^{2+} desensitizing sites, but the model (Swillens et al., 1998) is based on a limited set of data. Essentially, the various outcomes of these models point out to the need for continuous refinement in modeling the complex IP_3 regulation as more data are provided and the specific regulatory binding sites identified.

In addition, the different behavior of the channel in different membranes makes the results more confusing. It is

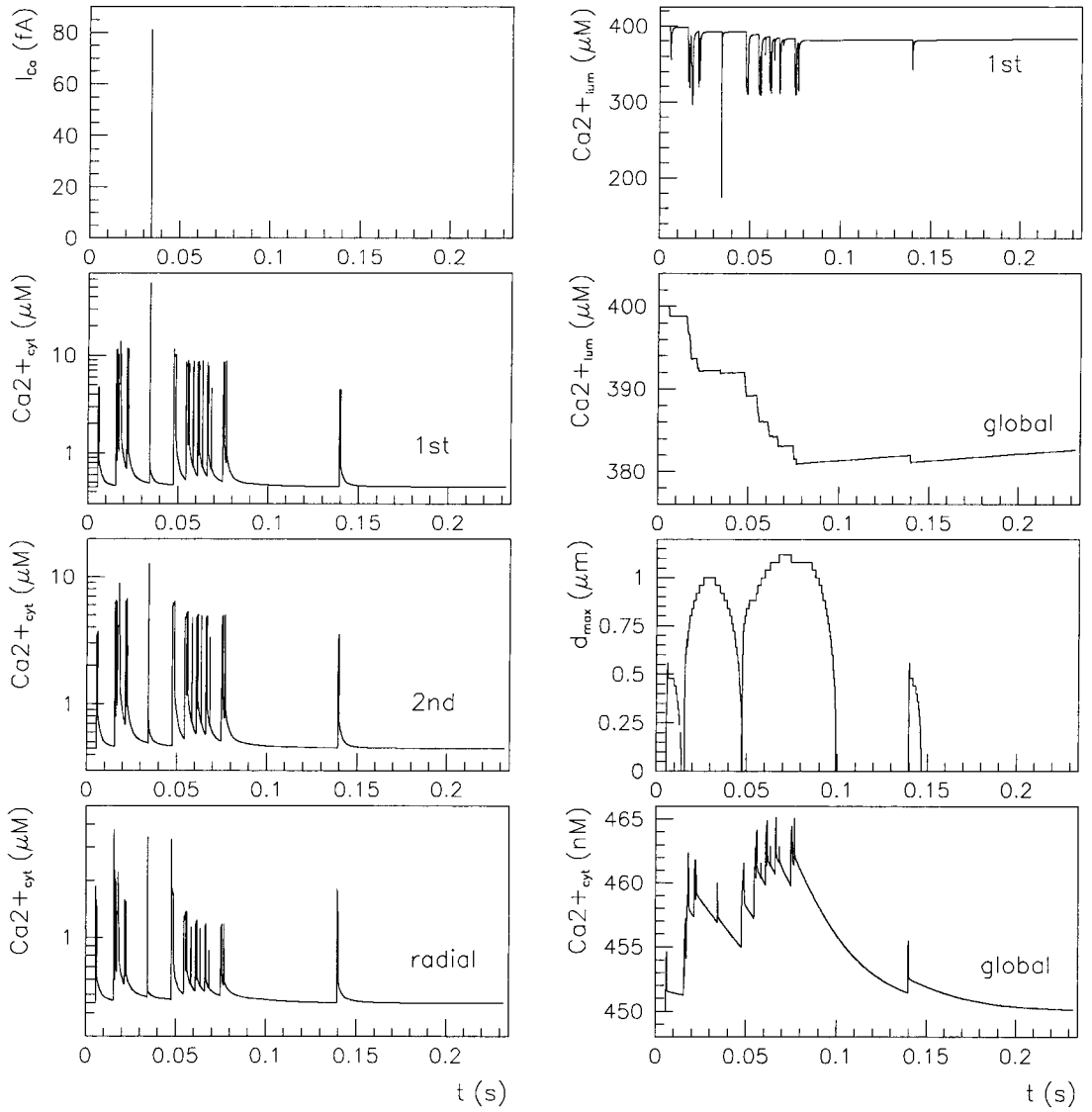

FIGURE 8 Fast calcium release dynamics simulated with nine-channel release site. Other conditions as in Fig. 7.

possible that reconstitution of the receptor into lipid bilayers alters the protein-protein and protein-lipid interactions and basically reduces by one order the magnitude of P_o. It would be interesting to know whether P_o at $[Ca^{2+}]_{cyt} \geq 50\ \mu M$ show inactivation at high IP_3 levels in bilayer experiments (see Fig. 6 in Moraru et al., 1999). If this would be the case, the dependence of P_o on Ca^{2+} and IP_3 could be explained by the same mechanism as proposed for the channel studied in the ER membrane. Here the data (Mak et al., 1998) indicate that two antagonist classes of Ca^{2+} binding sites exist and that Ca^{2+} binds to two monomers to open and to four monomers to close the channel. Moreover, IP_3 binding to the medium affinity site only seems to be implicated in regulation of channel activity, and it does so by attenuating the inhibitory effect of Ca^{2+}. Channel activity resumes to fast kinetics in excised membrane patches but spreads on a slow timescale in integral nuclear membrane, clearly showing loss of the slow component in the former case.

To describe the fast gating component of the ER Ca^{2+} channel, we assume it to be controlled by Ca^{2+} binding to an activating site, with a calculated Hill coefficient $\simeq 2$, by Ca^{2+} binding to an inhibitory site, with a calculated Hill coefficient $\simeq 3.2$, and by a hypothetical ligand (f_i) to account for the subunitary $P_{o,max}$ at the plateau domain of the $P_o(Ca^{2+})$ curve (Mak et al., 1998). We show that our model supports the ATP effect on channel activation by allosteric regulation with $K_d = 215\ \mu M$ and $h = 1.3$, similar to those deduced from a nonstandard Hill formula (Mak et al., 1999). It would be worth seeing whether the ATP binding site could have such low affinity for free ATP in the absence of Ca^{2+} as calculated here ($K_d \simeq 90\,mM$). Among the possible candidates as f_i ligands, only Ca^{2+}_{lum} comes in agreement with

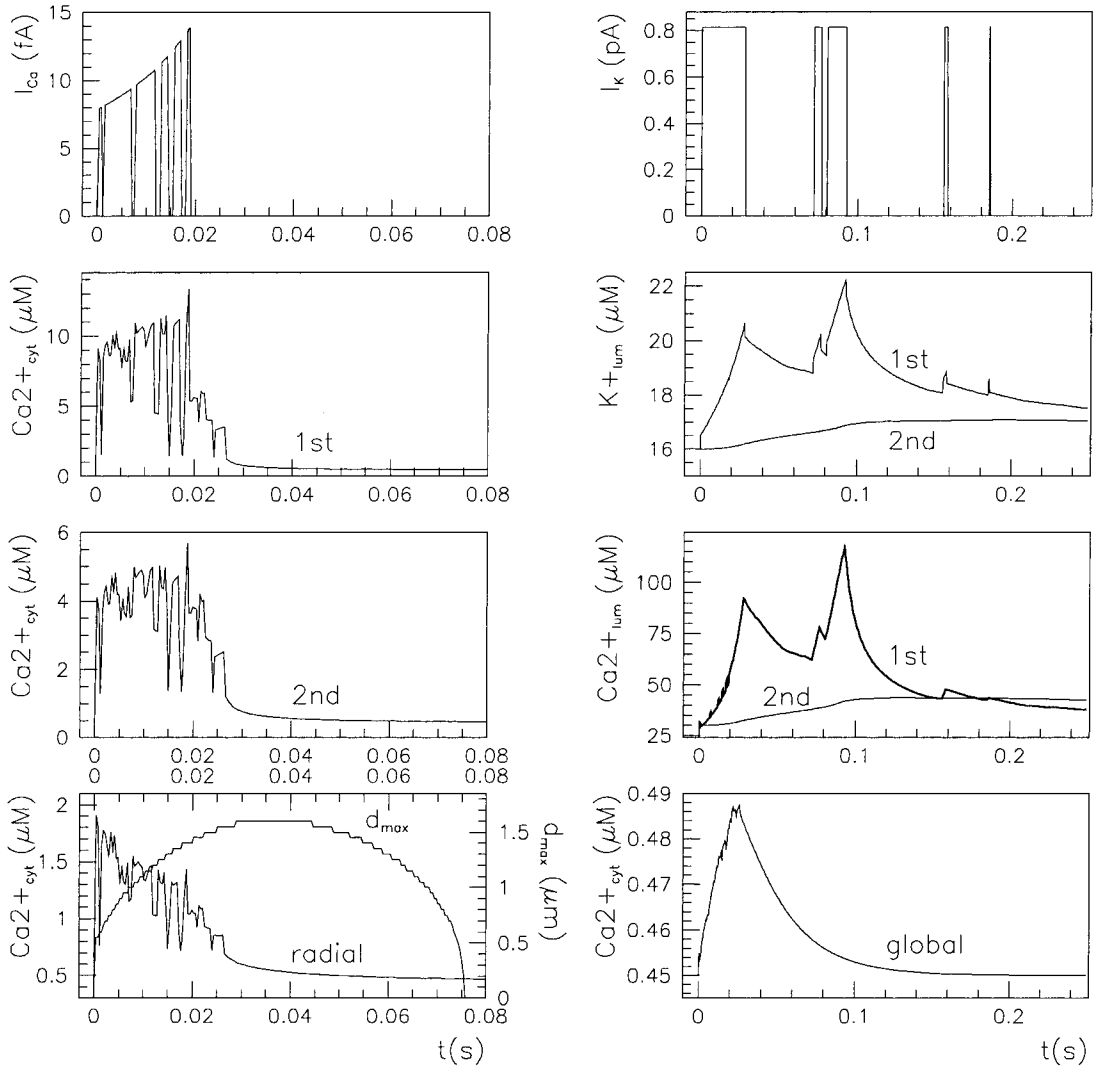

FIGURE 9 Fast calcium release at six-channel release site in conditions specified by Scenario I. The current through both Ca^{2+} and K^+ channel in the central element on the ER membrane are shown in the upper panels (I_{Ca} and I_K, respectively). Other notations as in Fig. 7. Over the simulated 250-ms period after IP_3 stimulation, calcium is released through the IP_3Rs cluster during the first 26 ms only. The stationary buffer level is 120 μM.

various data as analyzed with our model, but certainly more data are needed to define the exact mechanism of regulation.

Based on the results obtained here, we propose a number of possible mechanisms involved in calcium release regulation that fairly well describes many experimental data and observations, as follows:

1. The ER of cilliated cells is a huge reservoir of 4 M Ca^{2+} binding sites, most of which ($\simeq 90\%$) are masked by K^+, and a Ca^{2+} ion must compete with six K^+ ions inside the ER and with 11 K^+ ions inside the mucin granules of goblet cells.
2. Ca^{2+} has a high ($K_{dis} = 12$ nM) or a 50 times lower affinity for its activating site on the cytosolic side of the IP_3R, depending on whether ATP is bound or not.
3. Luminal Ca^{2+} might inhibit IP_3R activity with a low, possibly subunitary Hill coefficient.
4. Both comparison of data on IP_3R in excised versus intact nuclear membrane and calcium release simulations lend support for a three-module decomposition of channel gating, as follows: one fast, activating, controlled by cytosolic Ca^{2+} and ATP; one fast, inhibitory, controlled by cytosolic and luminal Ca^{2+}; and one slow, inactivating, controlled by cytosolic Ca^{2+} and IP_3.
5. Local calcium oscillations observed on a seconds scale in permeabilized cells might be driven by the slow inactivation of channels organized in discrete clusters composed of between six and 15 channels.
6. Out-of-phase calcium variations appear at rather constant luminal K^+ whereas sustained K^+ uptake by the lumen appears as a key factor in inducing parallel oscillations.
7. Different patterns of calcium signals, as seen in many experiments, can be induced depending on: Ca^{2+} and K^+

fluxes between ER and cytosol, intrinsic rapidity of Ca^{2+} and K^+ dissociation from the luminal matrix, and differences in channel distribution between cell types.

The model we propose here is the first to our knowledge that integrates in a quantitative manner the kinetic properties of the IP_3R with both the cytosolic and luminal calcium/potassium dynamics. On this basis we are able to reproduce various and puzzling aspects of calcium signaling observed in many experiments, as, for example, modest or large decreases (Barrero et al., 1997; Golovina and Blaustein, 1997) or increases (Golovina and Blaustein, 1997; Nguyen et al., 1998) in store filling after stimulation. So far, models for electrically excitable cells only could predict enhancement of calcium load during release.

Most important, our model can explain local calcium oscillations even in permeabilized cells, where intracellular calcium is not conserved. The nature of the allosteric transitions involved in the slow inactivation of the IP_3R (see Fig. 3 *B*) remains undefined, but may involve calmodulin (Patel et al., 1997; Missiaen et al., 1999) or IP_3 binding to its high affinity site (Kaftan et al., 1997; Moraru et al., 1999). An important prediction of the model is that $[Ca^{2+}]_{cyt}$ and $[Ca^{2+}]_{lum}$ variations result in- or out-of-phase if the ER transmembrane K^+ gradient is high or low, respectively (here if the chemical equilibrium in the store is attained at tens or hundreds of μM calcium, respectively). This could have interesting implications in producing distinct local calcium signals arising from distinct ER compartments (Golovina and Blaustein, 1997) or in calcium signaling in electrically excitable cells, where parallel evolutions are generally thought to develop as, for example, in pancreatic β-cells (Gilon et al., 1999). Nevertheless, many aspects of in vivo calcium release need further investigation. At present the data are not abundant and differences between cell types may lead to apparent discrepancies between various experimental results. However, the analysis here offers a more detailed description of the complex interplay between cytosolic and luminal control of calcium release, which undoubtedly has important effects on diverse calcium dependent processes, such as trigger of calcium influx through store-operated calcium channels (Hofer et al., 1998; Huang and Putney, 1998) birth and propagation of calcium waves (Dupont and Goldbeter, 1994; Lukyanenko et al., 1999), excitation-contraction coupling (Stern et al., 1997; Haddock et al., 1999), gene expression (Negulescu et al., 1994), or cell cycle progression (Baran, 1996).

APPENDIX 1: STEADY-STATE OPEN PROBABILITY

The four substates, denoted as $X_1 = (0,0)$, $X_2 = (0,1)$, $X_3 = (1,1)$, and $X_4 = (1,0)$, of each X-type gating module ($X = A$, activating, or $X = I$, inhibiting) are occupied at steady state with the probabilities:

$$P_{X1} = 1 - P_{X2} - P_{X3} - P_{X4} \tag{7}$$

$$P_{X2} = (\gamma_4^X - \gamma_2^X)/\delta^X \tag{8}$$

$$P_{X4} = (\gamma_1^X - \gamma_3^X)/\delta^X \tag{9}$$

$$P_{X3} = (P_{X2}\lambda_{23}^X + P_{X4}\lambda_{43}^X)/\lambda_3^X, \tag{10}$$

where

$$\gamma_1^X = \frac{\lambda_{21}^X}{\lambda_1^X} + \frac{\lambda_{23}^X}{\lambda_3^X} + 1 \tag{11}$$

$$\gamma_2^X = \frac{\lambda_{41}^X}{\lambda_1^X} + \frac{\lambda_{43}^X}{\lambda_3^X} + 1 \tag{12}$$

$$\gamma_3^X = \left(1 - \frac{\lambda_{34}^X}{\lambda_{14}^X}\right)\frac{\lambda_{23}^X}{\lambda_3^X} + 1 \tag{13}$$

$$\gamma_4^X = \frac{\lambda_4^X}{\lambda_{14}^X} + \left(1 - \frac{\lambda_{34}^X}{\lambda_{14}^X}\right)\frac{\lambda_{43}^X}{\lambda_3^X} + 1 \tag{14}$$

$$\delta^X = \gamma_1^X\gamma_4^X - \gamma_2^X\gamma_3^X, \tag{15}$$

provided $\delta^X \neq 0$. Here $\lambda_1^X = \lambda_{12}^X + \lambda_{14}^X$; $\lambda_3^X = \lambda_{32}^X + \lambda_{34}^X$; $\lambda_4^X = \lambda_{41}^X + \lambda_{43}^X$. λ_{ij}^X is the rate constant of the transition $X_i \rightarrow X_j$, $(i,j = 1, 4)$.

The "A" gate within the activating module is assumed open in both A_3 and A_4, whereas for the inhibitory module, the "I" gate is open in I_1 only. Each macrostate probability is obtained as the product of the partial probabilities of each of the two independent subsystems: $P(q_a,q_{fa},q_i,q_{fi}) = P(q_a,q_{fa}) \times P(q_i,q_{fi})$. The resulting steady-state open channel probability is then

$$P_o = (P_{A3} + P_{A4}) \times P_{I1}. \tag{16}$$

APPENDIX 2. DWELL-TIME DISTRIBUTIONS AND MISSED EVENTS

A representation of the possible state transitions is shown in Fig. 10. The open/close dwell-time histogram results from transitions from each of the open/closed states to a complementary state. The probability of the channel to leave any s state ($s = o$, open; $s = c$, closed) toward a certain state is constant (given by the rate constant of the respective transition), so:

1. The total number of events with duration τ is $n_s(\tau) = \sum_{j=1}^{m_s} N_{sj}\exp(-\lambda_{sj}\tau)$, with $N_{sj} = \alpha_{sj}N$ being the total number of events originating from the state s_j and N the total number of openings or, equivalently, closures of the channel during the recording time.
2. $\sum_{j=1}^{m_s} \alpha_{sj} = 1$.
3. The mean time spent in the s state $\tau_s = \sum_{j=1}^{m_s} \alpha_{sj}\tau_{sj}$.
4. $\tau_{sj}\tau_s^{-1} = P_{sj}P_s^{-1}$, where $\tau_{sj} = \lambda_{sj}^{-1}$.

λ_{sj} is the probability of leaving the s_j state toward a complementary s' state ($s' = c$ if $s = o$ and $s' = o$ if $s = c$) within 1 s; $m_o = 2$ the number of open states; and $m_c = 6$ the number of closed states that can switch directly to an open state. The weighting factors are:

$$\alpha_{sj} = \frac{P_sP_{sj}\lambda_{sj}}{\sum_{j=1}^{m_s} P_{sj}\sum_{j=1}^{m_s} P_{sj}\lambda_{sj}}, \tag{17}$$

$\lambda_{o1} = k_{a0}^{off} + k_{i0}^{on} + k_{fi0}^{on}$, and $\lambda_{o2} = k_a^{off} + k_{i0}^{on} + k_{fi0}^{on}$. The six components of the closed-state histogram are determined by the transitions: $C1$ ($\equiv A_2I_1$) $\rightarrow O_1$ ($\equiv A_3I_1$); $C2$ ($\equiv A_3I_2$) $\rightarrow O_1$; $C3$ ($\equiv A_3I_4$) $\rightarrow O_1$; $C4$ ($\equiv A_1I_1$) $\rightarrow O_2$ ($\equiv A_4I_1$); $C5$ ($\equiv A_4I_2$) $\rightarrow O_2$; and $C6$ ($\equiv A_4I_4$) $\rightarrow O_2$. The corresponding transition rates are: $\lambda_{c1} = k_{a0}^{on}$; $\lambda_{c2} = k_{i0}^{off}$; $\lambda_{c3} = k_{fi0}^{off}$; $\lambda_{c4} = k_a^{on}$; $\lambda_{c5} = k_{i0}^{off}$;

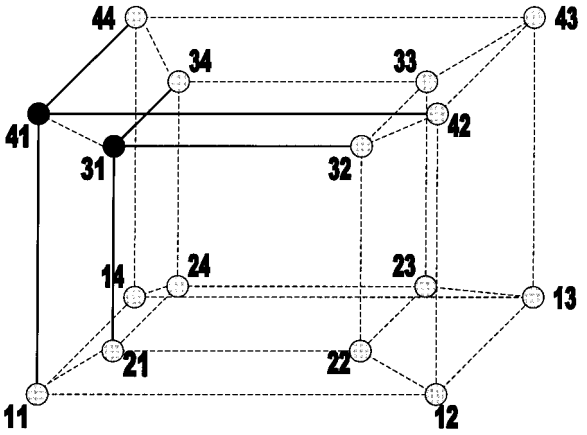

FIGURE 10 Sixteen-state representation of the IP_3R's fast kinetics. Each A_{j_A} I_{j_I} state is labeled by the pair $j_A j_I$, with j_X representing the current of the four possible substates within the X module. Open and closed states are marked by black and gray circles, respectively. Possible transitions between open states and their neighbor closed states are highlighted.

and $\lambda_{c6} = k_{fi0}^{off}$. The A_{j_A} I_{j_I} state probability equals $P_{A_{j_A}}$ $P_{I_{j_I}}$, calculated with the aid of Eqs. 7–15.

To calculate the errors introduced by missed events during channel recording (see also Colquhoun et al., 1996), we estimate the distortion of P_o, τ_o, and τ_c caused by successions of up to four undetectable events. An event with duration lower than the time detection limit τ_d is assumed to appear with the same probability all over the recording. The number of detected events reduces to $N^* = N(\varepsilon_o + \varepsilon_c - 1)$, provided $\varepsilon_o + \varepsilon_c > 1$. Here $\varepsilon_s = \sum_{j=1}^{m_s} \alpha_{sj}\varepsilon_{sj}$, with $\varepsilon_{sj} = \exp(-\lambda_{sj}\tau_d)$. Part of the s-type missed events contribute to the apparent s' state total time, so that the measured mean open/close time can be approximated as:

$$\tau_s^* = (\tau_s - \Delta\tau_{ss'} + \Delta\tau_{s's})N/N^* \tag{18}$$

$$\begin{aligned}\Delta\tau_{ss'} &= \beta_s \sum_{j=1}^{m_s} \alpha_{sj}\lambda_{sj}\int_0^{\tau_d} te^{-\lambda_{sj}t}dt \\ &= \varepsilon_s(1-\varepsilon_{s'})(1-\varepsilon_s^2\varepsilon_{s'}^2)\sum_{j=1}^{m_s}\alpha_{sj}\tau_{sj}\left[1-\left(1+\frac{\tau_d}{\tau_{sj}}\right)\varepsilon_{sj}\right],\end{aligned} \tag{19}$$

where $\beta_s = \sum_{j=1}^{4} N_{js}^{nd}/N$ is the fraction of s undetectable events recorded as prolongation of an s' regular event, and $N_{1s}^{nd} = N(1-\varepsilon_{s'})^2\varepsilon_s$, $N_{2s}^{nd} = N(1-\varepsilon_{s'})\varepsilon_s\varepsilon_{s'}(1-\varepsilon_s)$, $N_{3s}^{nd} = N(1-\varepsilon_{s'})^2\varepsilon_s^2\varepsilon_{s'}$, and $N_{4s}^{nd} = N(1-\varepsilon_{s'})\varepsilon_s^2\varepsilon_{s'}^2(1-\varepsilon_s)$. Then the measured $P_o^* = \tau_o^*/(\tau_c^*+\tau_o^*)$. The reliability of this approach was tested with stochastic simulations of each regulatory site occupancy and count of specific events over a period ≥500 s. Average values from 10 different simulations were in good agreement with the theoretical ones for all quantities (N, N^*, τ_o, τ_o^*, τ_c, τ_c^*, P_o, and P_o^*) with any set of parameters used.

APPENDIX 3: SIMULATION PROCEDURE

We discretized the Laplacian operator in cylindrical geometry. The equations for the mobile species evolution were numerically solved according to an explicit finite difference formula, accurate to order $(\Delta r)^2$, $(\Delta z)^2$, $(\Delta\phi)^2$, and Δt. We have checked that for the immobile species, the diffusion constrained time step is sufficiently small to yield virtually the same results if using either a first-order or fourth-order solving method. From the geometrical point of view, we consider an ER tubule segment as a cylinder of radius r_T, symmetrically surrounded by a cytosolic volume of depth r_C. The total simulated volume is then a cylinder of radius $r_T + r_C$ and length z_T, divided into $n_\phi \times n_z \times (n_{r_T} + n_{r_C})$ elements, where $n_x = x_{max}/\Delta x$ for each cylindrical coordinate x (i.e., r, ϕ, or z). At the ER-cytosol boundary (ECB), we consider a cluster of N_{Ca} calcium, and other of N_K potassium, equally spaced channels, positioned symmetrically against the planes $z = z_T/2$ and $\phi = 0$. The interchannel distance is assumed to be d. Then, for space discretization, the angular increment is taken as $\Delta\phi = d/r_T$, whereas the radial and longitudinal steps are $\Delta r = \Delta z = d$. The running code was implemented in Fortran language on either UNIX or VAX workstations. It routinely solves a number of $n_\phi \times n_z \times [n_{r_T} \times (3\,\text{PDE}+2\,\text{ODE})_{lumen} + n_{r_C} \times (3\,\text{PDE}+1\,\text{ODE})_{cytosol}]$ partial (PDE) and ordinary (ODE) differential equations by updating all variables at every instant.

Single channel ionic currents are considered of the form

$$I_X(\phi,z) = \min[I_X^N(\phi,z), I_X^{sat}(\phi,z)], \tag{20}$$

where

$$I_X^N(\phi,z) = \frac{g_X RT}{z_X F} \times \ln\left[\frac{Y_X(r_T - \Delta r/2,\phi,z)}{Y_X(r_T + \Delta r/2,\phi,z}\right] \tag{21}$$

is the local Nernst potential-driven current and

$$I_X^{sat}(\phi,z) = 2\pi z_X F D_X r_X^{cp} Y_X \times 10^{-3} \tag{22}$$

is the diffusion-limited saturating channel current (Hille, 1992). Here the symbols are: X, ion type (Ca^{2+} or K^+); D_X, diffusion coefficient; g_X, single channel conductance; z_X, ion valence; R, gas constant; T, temperature; F, Faraday constant; Y_X, local concentration of X ions; and r_X^{cp} the capture radius of the pore (nevertheless it may depend also on nongeometric factors involving ion diffusion at the channel mouth). In taking I_X of the form given in Eq. 20, we assumed the ER membrane potential is zero, as electroneutrality is currently considered both at rest and during calcium release. We also used a nonequilibrium formula for I_X, given by ion binding to a single site inside the channel during permeation (Hille, 1992), with qualitatively similar results. This, however, requires the introduction of several arbitrary kinetic parameters.

Gating of each apamin-sensitive ASK channel is assumed to be driven by opening of one single gate by calcium binding to one site, with Hill coefficient $h_{ASK} = 4$, apparent dissociation constant $K_{ASK} = 1\ \mu M$ (Vergara et al., 1998), and off-rate constant $k_{ASK}^{off} = 150 - 500\,s^{-1}$ in agreement with specific experimental data (Marrion and Tavalin, 1998). For both calcium and potassium channels, stochastic simulations of each regulatory site occupancy are performed by generating, at every time step, a random number and comparing it to the product between the corresponding transition rate and the time step Δt.

Neumann conditions are introduced at the ECB according to the fluxes crossing each elementary ER membrane patch, among which the Ca^{2+}-ATPase driven flux, $J_{Ca}^{pump} = J_{max}^{pump} \times [Ca^{2+}]_{cyt}^2/([Ca^{2+}]_{cyt}^2 + K_P^2)$, is supposed to be permanent and uniformly distributed on the tubule surface. At $r = r_C + r_T$, Dirichlet (constant concentration) conditions were used as specified, whereas at $z = 0$, z_T, and $\phi = 0$, 2π, periodic, and at $r = 0$, no-flux, boundary conditions were assumed. Periodicity at the z edges is equivalent to considering a uniform distribution of identical, synchronized (Horne and Meyer, 1997) release sites (clusters) along a continuous ER tubule spanning the cytosol over a distance $\gg z_T$ and assumed in no vicinity to other tubules over a distance $2r_C$, as experimentally shown (Callamaras and Parker, 1999) for ~25% of puffs evoked by subthreshold stimuli, if the tubule orientation is considered here parallel to the plasma membrane. Local concentrations are determined by calculating the radial average at $z = z_T/2$ and $\phi = 0$ (the radial direction through the center of the cluster), over the distance where $[Ca^{2+}]_{cyt}(r, \phi, z, t)$ exceeds by a measurable difference (Swillens et al., 1998) of 20 nM the basal level (which is fixed by the concentration in the medium). Global concentrations were calculated over the luminal and cytosolic simulated volume. In all our simulations, ER concentrations resulted practically uniform along the tubule over 0.2 s, and variations in

global cytosolic Ca^{2+} followed exactly the variations in the local concentration, about one order of magnitude lower. All concentrations are averaged every 0.2 s (Nguyen et al., 1998). J_{max}^{pump} was calculated at every simulation from the condition of equilibrium between total calcium outflow and pump flux at rest.

The spatio-temporal evolution of each mobile specie concentration (Y_m) is calculated according to the reaction-diffusion equation:

$$\frac{\partial Y_m(r,\phi,z,t)}{\partial t} = D_m \nabla^2 Y_m(r,\phi,z,t) + F_Y(r,\phi,z,t), \quad (23)$$

where $F_Y(r, \phi, z, t)$ is the buffer exchange term. Sources and removal terms are only considered at the ECB and introduced explicitly in the flux boundary conditions. Inside the store, the two mobile species considered are Ca^{2+} and K^+, and the buffering terms are given by Eqs. 3 and 4, respectively. In the cytosol, we determine the evolution of three mobile species, namely Ca^{2+}, K^+, and the exogenous calcium mobile buffer EGTA (the endogenous mobile buffer is lost by permeabilization). Cytosolic calcium buffering is calculated with a stoichiometry 1:1 for all buffers, for a total concentration of fix endogenous buffer sites $B_{T,fix}$ or mobile, exogenous $B_{T,mob}$, without making any buffering approximation. For the mobile buffer and free cytosolic calcium the buffer exchange term is

$$\begin{aligned} &F_{B,mob}(r,\phi,z,t) \\ &= F_{Ca,cyt}(r,\phi,z,t) \\ &= -k_{B,mob}^{on} \times [Ca^{2+}]_{cyt}(r,\phi,z,t) \times [B_{mob}](r,\phi,z,t) \\ &\quad + k_{B,mob}^{off} \times [B_{mob}Ca](r,\phi,z,t), \end{aligned} \quad (24)$$

with $k_{B,mob}^{on} = k_{B,mob}^{off}/K_{B,mob}$, where $K_{B,mob}$ is the respective dissociation constant. The evolution of fix species is determined within the lumen from Eqs. 1 and 2 and within the cytosol from

$$\begin{aligned} \frac{d[B_{fix}](r,\phi,z,t)}{dt} &= -k_{B,fix}^{on} \times [Ca^{2+}]_{cyt}(r,\phi,z,t) \times [B_{fix}](r,\phi,z,t) \\ &\quad + k_{B,fix}^{off} \times [B_{fix}Ca](r,\phi,z,t), \end{aligned} \quad (25)$$

with $k_{B,fix}^{on} = k_{B,fix}^{off}/K_{B,fix}$. Here again, $K_{B,fix}$ is the dissociation constant of the complex $B_{fix}Ca$. If spatial uniformity is assumed at the initial moment, the conservation rule

$$[B_{mob/fix}](r,\phi,z,t) + [B_{mob/fix}Ca](r,\phi,z,t) = B_{T,mob/fix} \quad (26)$$

holds at every instant (Naraghi and Neher, 1997), which reduces the number of equations by two in each spatial element.

The time step $\Delta t = 0.75-1$ μs was optimized separately before every simulation and numerically tested on a 0.5-s interval to detect instabilities. The highest sensitivity to Δt was met by $[K^+]$ at the "center" of the ER tubule (the first radial iteration). During all simulations, K^+ in all central elements was continuously checked to remain below 160 mM. The spatial increment was kept in the range $\Delta r = 35-50$ nm. Simulation standard parameter values are given in Table 2.

REFERENCES

Atri, A., J. Amundson, D. Clapham, and J. Sneyd. 1993. A single-pool model for intracellular calcium oscillations and waves in the *Xenopus laevis* oocyte. *Biophys. J.* 65:1727–1739.

Baran, I. 1996. Calcium and cell cycle progression: possible effects of external perturbation on cell proliferation. *Biophys. J.* 70:1198–1213.

Barrero, M. J., M. Montero, and J. Alvarez. 1997. Dynamics of $[Ca^{2+}]$ in the endoplasmic reticulum and cytoplasm in intact HeLa cells. *J. Biol. Chem.* 272:27694–27699.

Berridge, M. J. 1993. Inositol trisphosphate and calcium signaling. *Nature.* 361:315–325.

Berridge, M. J., P. Lipp, and M. D. Bootman. 2000. The versatility and universality of calcium signalling. *Nature Rev. Mol. Cell Biol.* 1:11–21.

Bezprozvanny, I., and B. E. Erlich. 1994. Inositol (1,4,5)-trisphosphate ($InsP_3$)-gated Ca channels from cerebellum: conduction properties for divalent cations and regulation by intraluminal calcium. *J. Gen. Physiol.* 104:821–856.

Bezprozvanny, I., J. Watras, and B. E. Erlich. 1991. Bell-shaped calcium response curves of $Ins(1,4,5)P_3$- and calcium-gated channels from endoplasmic reticulum of cerebellum. *Nature.* 351:751–754.

Callamaras, N., and I. Parker. 1999. Radial localization of inositol 1,4,5-trisphosphate-sensitive Ca^{2+} release sites in *Xenopus* oocytes resolved by axial confocal linescan imaging. *J. Gen. Physiol.* 113:199–213.

Clapham, D. E. 1995. Calcium signaling. *Cell.* 80:259–268.

Colquhoun, D., A. G. Hawkes, and K. Srodzinski. 1996. Joint distributions of apparent open and shut times of single-ion channels and maximum likelihood fitting of mechanisms. *Philos. Trans. R. Soc. Lond.* A354:2555–2590.

De Young, G. W., and J. Keizer. 1992. A single-pool inositol 1,4,5-trisphosphate-receptor-based model for agonist-stimulated oscillations in Ca^{2+} concentration. *Proc. Natl. Acad. Sci. USA.* 89:9895–9899.

Dupont, G. 1999. Spatio-temporal organization of cytosolic Ca^{2+} signals: from experimental to theoretical aspects. *Comments Theor. Biol.* 5:305–340.

Dupont, G., and A. Goldbeter. 1994. Properties of intracellular Ca^{2+} waves generated by a model based on $Ca(^{2+})$-induced Ca^{2+} release. *Biophys. J.* 67:2191–2204.

Finch, E. A., T. J. Turner, and S. M. Goldin. 1991. Calcium as a coagonist of inositol 1,4,5-trisphosphate-induced calcium release. *Science.* 252:443–446.

Gilon, P., A. Arredouani, P. Gailly, J. Gromada, and J. C. Henquin. 1999. Uptake and release of Ca^{2+} by the endoplasmic reticulum contribute to the oscillations of the cytosolic Ca^{2+} concentration triggered by Ca^{2+} influx in the electrically excitable pancreatic B-cells. *J. Biol. Chem.* 274:20197–20205.

Golovina, V. A., and M. P. Blaustein. 1997. Spatially and functionally distinct Ca^{2+} stores in sarcoplasmic and endoplasmic reticulum. *Science.* 275:1643–1648.

Györke, I., and S. Györke. 1998. Regulation of the cardiac ryanodine receptor channel by luminal Ca^{2+} involves luminal Ca^{2+} sensing sites. *Biophys. J.* 75:2801–2810.

Haddock, P. S., W. A. Coetzee, E. Cho, L. Porter, H. Katoh, D. M. Bers, M. S. Jafri, and M. Artman. 1999. Subcellular $[Ca^{2+}]_i$ gradients during excitation-contraction coupling in newborn rabbit ventricular myocytes. *Circ. Res.* 85:415–427.

Hajnóczky, G., R. Hager, and A. P. Thomas. 1999. Mitochondria suppress local feedback activation of inositol 1,4,5-trisphosphate receptors by Ca^{2+}. *J. Biol. Chem.* 274:14157–14162.

Hajnóczky, G., and A. P. Thomas. 1994. The inositol trisphosphate calcium channel is inactivated by inositol trisphosphate. *Nature.* 370:474–477.

Hille, B. 1992. Ionic Channels of Excitable Membranes. Sinauer Associates, Sunderland, MA.

Hofer, A. M., C. Fasolato, and T. Pozzan. 1998. Capacitive Ca^{2+} entry is closely linked to the filling state of internal Ca^{2+} stores: a study using simultaneous measurements of I_{CRAC} and intraluminal Ca^{2+}. *J. Cell Biol.* 140:325–334.

Horne, J. H., and T. Meyer. 1997. Elementary calcium release units induced by inositol trisphosphate. *Science.* 276:1690–1693.

Huang, Y., and J. W. Putney, Jr. 1998. Relationship between intracellular calcium store depletion and calcium release-activated calcium current in a mast cell line (RBL-1). *J. Biol. Chem.* 273:19554–19559.

Kaftan, E. J., B. E. Ehrlich, and J. Watras. 1997. Inositol 1,4,5-trisphosphate and calcium interact to increase the dynamic range of

$InsP_3$ receptor-dependent calcium signaling. *J. Gen. Physiol.* 110:529–538.

Kim, J. H., L. Johannes, B. Goud, C. Antony, C. A. Lingwood, R. Daneman, and S. Grinstein. 1998. Noninvasive measurement of the pH of the endoplasmic reticulum at rest and during calcium release. *Proc. Natl. Acad. Sci. USA*. 95:2997–3002.

Lukyanenko, V., S. Subramanian, I. Györke, T. F. Wiesner, and S. Györke. 1999. The role of luminal Ca^{2+} in the generation of Ca^{2+} waves in rat ventricular myocytes. *J. Physiol.* 518:173–186.

Mak, D. O., and J. K. Foskett. 1997. Single-channel kinetics, inactivation, and spatial distribution of inositol (1,4,5) trisphosphate (IP_3) receptor in *Xenopus* oocyte nucleus. *J. Gen. Physiol.* 109:571–587.

Mak, D. O., S. McBride, and J. K. Foskett. 1998. Inositol 1,4,5-trisphosphate activation of inositol 1,4,5-trisphosphate receptor Ca^{2+} channel by ligand tuning of Ca^{2+} inhibition. *Proc. Natl. Acad. Sci. USA*. 95:15821–15825.

Mak, D. O., S. McBride, and J. K. Foskett. 1999. ATP regulation of type 1 inositol 1,4,5-trisphosphate receptor channel gating by allosteric tuning of Ca^{2+} activation. *J. Biol. Chem.* 274:22231–22237.

Marrion, N. V., and S. J. Tavalin. 1998. Selective activation of Ca^{2+}-activated K^+ channels by co-localized Ca^{2+} channels in hippocampal neurons. *Nature*. 395:900–905.

Marshall, I. C. B., and C. W. Taylor. 1993. Regulation of inositol 1,4,5-trisphosphate receptors. *J. Exp. Biol.* 184:161–182.

Mignery, G. A., P. A. Johnston, and T. C. Sudhof. 1992. Mechanism of Ca^{2+} inhibition of inositol 1,4,5-trisphosphate ($InsP_3$) binding to the cerebellar $InsP_3$ receptor. *J. Biol. Chem.* 267:7450–7455.

Missiaen, L., J. B. Parys, A. F. Weidema, H. Sipma, S. Vanlingen, P. De Smet, G. Callewaert, and H. De Smedt. 1999. The bell-shaped Ca^{2+} dependence of the inositol 1,4,5-trisphosphate-induced Ca^{2+} release is modulated by Ca^{2+}/calmodulin. *J. Biol. Chem.* 274: 13748–13751.

Mitchell, R. D., H. K. B. Simmerman, and L. R. Jones. 1988. Ca^{2+} binding effects on protein conformation and protein interactions of canine cardiac calsequestrin, *J. Biol. Chem.* 263:1376–1381.

Moraru, I. I., E. J. Kaftan, B. E. Ehrlich, and J. Watras. 1999. Regulation of type 1 inositol 1,4,5-trisphosphate-gated calcium channels by $InsP_3$ and calcium. *J. Gen. Physiol.* 113:837–849.

Naraghi, M., and E. Neher. 1997. Linearized buffered Ca^{2+} diffusion in microdomains and its implication for calculation of [Ca^{2+}] at the mouth of a calcium channel. *J. Neurosci.* 17:6961–6973.

Negulescu, P. A., N. Shastri, and M. D. Cahalan. 1994. Intracellular calcium dependence of gene expression in single T lymphocytes. *Proc. Natl. Acad. Sci. USA*. 91:2873–2877.

Nguyen, T., W. C. Chin, and P. Verdugo. 1998. Role of Ca^{2+}/K^+ ion exchange in intracellular storage and release of Ca^{2+}. *Nature*. 395:908–912.

Oancea, E., and T. Meyer. 1996. Reversible desensitization of inositol trisphosphate-induced calcium release provides a mechanism for repetitive calcium spikes. *J. Biol. Chem.* 271:17253–17260.

Parker, I., and I. Ivorra. 1990. Inhibition by Ca^{2+} of inositol trisphosphate-mediated Ca^{2+} liberation: a possible mechanism for oscillatory release of Ca^{2+}. *Proc. Natl. Acad. Sci. USA*. 87:260–264.

Pape, P. C., D. S. Jong, and W. K. Chandler. 1995. Calcium release and its voltage dependence in frog cut muscle fibers equilibrated with 20 mM EGTA. *J. Gen. Physiol.* 106:259–336.

Patel, S., S. A. Morris, C. E. Adkins, G. O'Beirne, and C. W. Taylor. 1997. Ca^{2+}-independent inhibition of inositol trisphosphate receptors by calmodulin: as a possible means of regulating Ca^{2+} mobilization. *Proc. Natl. Acad. Sci. USA*. 94:11627–11632.

Sachs, F., F. Qin, and P. Palade. 1995. Models of Ca^{2+} release channel adaptation. *Science*. 267:2010–2011.

Sienaert, I., H. De Smedt, J. B. Parys, L. Missiaen, S. Vanlingen, H. Sipma, and R. Casteels. 1996. Characterization of a cytosolic and a luminal Ca^{2+} binding site in the type I inositol 1,4,5-trisphosphate receptor. *J. Biol. Chem.* 271:27005–27012.

Sienaert, I., L. Missiaen, H. De Smedt, J. B. Parys, H. Sipma, and R. Casteels. 1997. Molecular and functional evidence for multiple Ca^{2+}-binding domains in the type 1 inositol 1,4,5-trisphosphate receptor. *J. Biol. Chem.* 272:25899–25906.

Stern, M. D., G. Pizzaro, and E. Rios. 1997. Local control model of excitation-contraction coupling in skeletal muscle. *J. Gen. Physiol.* 110:415–440.

Swillens, S., P. Champeil, L. Combettes, and G. Dupont. 1998. Stochastic simulation of a single inositol 1,4,5-trisphosphate-sensitive Ca^{2+} channel reveals repetitive openings during 'blip-like' Ca^{2+} transients. *Cell Calcium*. 23:291–302.

Swillens, S., G. Dupont, L. Combettes, and P. Champeil. 1999. From calcium blips to calcium puffs: theoretical analysis of the requirements for interchannel communication. *Proc. Natl. Acad. Sci. USA*. 96:13750–13755.

Taylor, C. W., and D. Traynor. 1995. Calcium and inositol trisphosphate receptors. *J. Membr. Biol.* 145:109–118.

Thrower, E. C., H. Mobasheri, S. Dargan, P. Marius, E. J. A. Lea, and A. P. Dawson. 2000. Interaction of luminal calcium and cytosolic ATP in the control of type 1 inositol (1,4,5) trisphosphate receptor channels. *J. Biol. Chem.* 275:36049–36055.

Vergara, C., R. Latorre, N. V. Marrion, and J. P. Adelman. 1998. Calcium-activated potassium channels. *Curr. Opin. Neurobiol.* 8:321–329.